Hindawi
Mathematical Problems in Engineering
Volume 2019, Article ID 3960864, 24 pages
https://doi.org/10.1155/2019/3960864

Research Article

Influence of Backfill Compaction on Mechanical Characteristics of High-Density Polyethylene Double-Wall Corrugated Pipelines

Hongyuan Fang[1,2,3], **Peiling Tan**[1,2,3], **Bin Li**[1,2,3], **Kangjian Yang**[1,2,3] and **Yunhui Zhang**[1,2,3]

[1]*School of Water Conservancy and Engineering, Zhengzhou University, Zhengzhou 450001, China*
[2]*National Local Joint Engineering Laboratory of Major Infrastructure Testing and Rehabilitation Technology, Zhengzhou 450001, China*
[3]*Collaborative Innovation Center of Water Conservancy and Transportation Infrastructure Safety, Henan Province, Zhengzhou 450001, China*

Correspondence should be addressed to Peiling Tan; tpl1752311002@163.com

Received 23 June 2019; Revised 16 September 2019; Accepted 3 October 2019; Published 31 October 2019

Academic Editor: Emilio Turco

Copyright © 2019 Hongyuan Fang et al. This is an open access article distributed under the Creative Commons Attribution License, which permits unrestricted use, distribution, and reproduction in any medium, provided the original work is properly cited.

For flexible pipelines, the influence of backfill compaction on the deformation of the pipe has always been the focus of researchers. Through the finite element software, a three-dimensional soil model matching the exterior wall corrugation of the high-density polyethylene pipe was skillfully established, and the "real" finite element model of pipe-soil interaction verified the accuracy through field test. Based on the model, the strain distribution at any position of the buried HDPE pipe can be obtained. Changing the location and extent of the loose backfill, the strain and radial displacement distributions of the interior and exterior walls of the HDPE pipe under different backfill conditions when external load applied to the foundation were analyzed, and the dangerous parts of the pipe where local buckling and fracture may occur were identified. It is pointed out that when the backfill is loose, near the interface between the backfill loose region and the well-compacted region, the maximum circumferential strain occurs frequently, the exterior wall strain is more likely to increase greatly on the region near crown or invert, the interior wall strains increase in amplitude at springline, and the location of the loose region has a greater influence on the strain of the pipe than the size of the loose area.

1. Introduction

High-density polyethylene (HDPE) double-corrugated pipe is widely used in the municipal engineering for significant advantages such as chemical resistance, light weight, and simple construct. The special profile of pipe featured with the smooth interior wall, and the corrugated exterior wall makes the ring stiffness much higher than that of the straight wall pipes of the same diameter and thickness. Figure 1 shows the cross section of pipe walls and defines the terminology in different locations of the profile (Figure 1).

The Chinese specification (Buried plastic drainage pipe construction) uses the normalized deflection by diameter to evaluate the pipe deformation [1]; the pipe strains and local profile stability are not considered. However, under the long-term external load, the tensions and compressions may follow the stress cracking and ductile failure, respectively. The special profile makes the strain distribution in different locations of the HDPE pipes more complicated; the local bucking of the slender elements of the profile may be caused by special strain distribution [2].

There are two directions for the study of the deformation of pipes, one is the influence of accidental factors on the deformation of pipelines, such as ground overload [3, 4], ground subsidence [5–7], blasting [8, 9], and rockfall impact [10, 11]; and the other is the influence of long-term state on pipes, such as installation conditions [12, 13], long-term vehicular load [14, 15], fault displacement [16], and

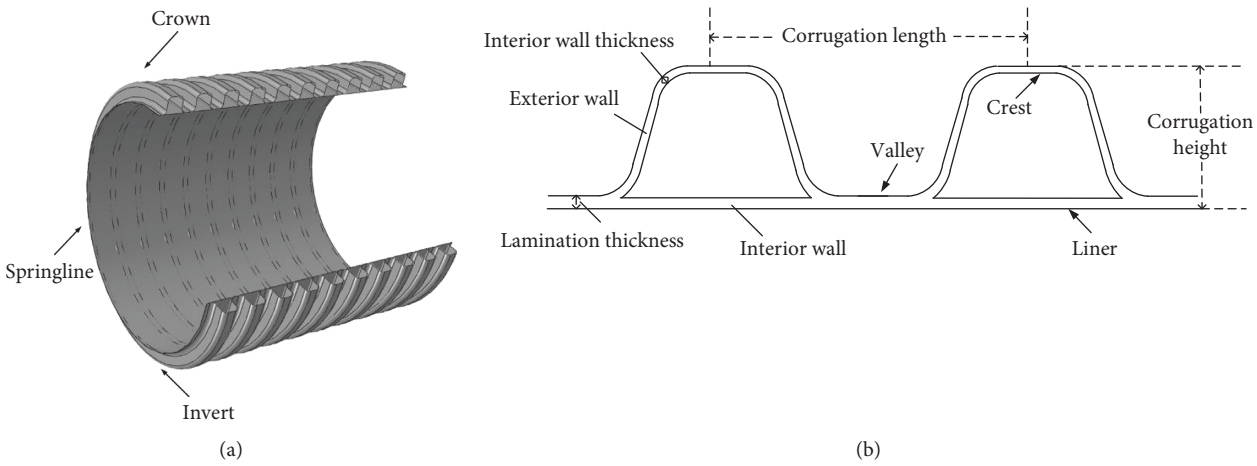

Figure 1: Profile of pipes: (a) section through pipes; (b) cross section of pipe walls.

foundation pit excavation [17, 18]. The HDPE pipes are classical embedded flexible pipes, and the soil-pipe interaction will control pipe deformation under external load, so researchers focus on the impact of long-term installation state on the deformation of HDPE pipe. The soil arching developed in the soil cover depends on the stiffness of the pipes and on the stiffness of the backfill soil surrounding the pipes (based on the degree, water content, soil material, and grade). In addition, the backfill configuration and the method of compaction can also have an impact on the nature of the load and support the pipes [19]. A survey had been performed to evaluate the field performance of the existing HDPE pipes. It was found that the low-degree compaction and low-grade backfill material will lead to excessive deformation and failure of the shallow-embedded pipes [20]. Therefore, it was urgent and necessary to study the influence of the backfill compaction on the pipe strain. A lot of theoretical design methods, tests, and numerical simulations about the flexible pipes were carried out by scholars.

Based on the theory of granular limit equilibrium and in view of the influence of the pipe diameter and the trench width, Marston and Anderson derived the formula for calculating the vertical earth pressure of the embedded pipe [21]. Spangler and Shafer studied the structural performance of the flexible pipe and proposed a design formula for the horizontal deflection of the flexible pipe, symbolizing that a rational theory of design has been developed [22]. Howard compared the experimental values with the predicted values of Spangler equation, and the results showed that the deflection experimental values of PVC pipe were much lower than the predicted values when the compaction of backfill soil was loose [23].

Faragher et al. explored the axial strains of the plastic pipes in installation when changing the compaction degree of the sand or the gravel backfill material by laboratory testing [24]. Sargand et al. carried out a full-scale field test to investigate the behaviour of the embedded plastic pipes with different installation parameters (backfill material, compaction degree, and bedding thickness) [25]. Laboratory and full-scale field tests were conducted by McGrath et al. to study the soil behaviour during installation; variables include pipe types (concrete, steel, and plastic) and dimensions, field ground conditions, trench width, backfill method, and compaction degree. The results showed that the relatively small change of the backfill density has a significant impact on the backfill stiffness, and all the parameter variables of the backfill process have a significant impact on the behaviour of the pipes [26].

Through the laboratory test and FEM, Dhar et al. recommended the two-dimensional finite element analysis, which could be used effectively to calculate pipe deflections; they also applied FEM to study the effect of a soft haunch region on the strains in profiled thermoplastic pipes [27]. Using ABAQS, Al-Abri and Mohamedzein investigated a similar problem; a two-dimensional finite element model was established to evaluate the deformation of HDPE and PVC pipes when the compactness of the sandy backfill was changed [28]. Wang et al. studied the earth pressure variation and HDPE pipe deflection with the height of fine-grained soils backfill, and proposed an empirical equation to relate the ratio of the vertical deflection to the horizontal deflection and the soil cover thickness [29].

Vehicular load is the external load that municipal buried pipes must consider. The deformation of pipes had been reported by researchers when the vehicular load was applied to the ground as an external load.

McGrath et al. measured the stress and deformation of a large-diameter shallow-embedded HDPE pipe under the real vehicular load through a full-scale field study [30]. Noor and Dhar studied the pipe-soil interaction under a vehicle load by using ANSYS and established a three-dimensional pipe-soil model [31]. Through a laboratory model test, Tafreshi and Khalaj used repeated load to simulate the vehicle load and changed the parameters such as buried depth, sand backfill density, and intensity of load and also studied the settlement of the soil surface and the pipe radial deformations [32].

The distribution of HDPE pipe strains and deflection when the backfill degree of compaction was not according to the specification was reported by test and the two-

dimensional finite element model; the three-dimensional finite soil-pipe model was not used to simulate the effect of backfill parameters on the pipe response. Therefore, it is necessary to establish a three-dimensional model of the HDPE pipe and study the effect of the compactness of the backfill on the strain and deformation of the pipe.

The objective of this paper is to set up a real three-dimensional finite element model of HDPE double-wall corrugated pipe and soil and provide a theoretical basis for studying the strain distribution and deformation of pipe when the compactness of the backfill soil changes. The validity of the three-dimensional model is verified by comparing the numerical strain with the measured strain collected through the full-scale test. Based on the numerical model, it is analyzed the effects of the loose backfill of different regions on pipe under the vehicular loads.

2. Field Installation of Flexible Pipes

2.1. Description of Flexible Pipes and Strain Gauges. The HDPE double-wall corrugate pipe with the length of 6.0 m was investigated in this field-test program, and the nominal diameter is 800 mm. The pipe geometries and material properties are shown in Table 1. Before pipe installation, the electrical resistance gauges (BQ120-80AA-P200, accurate within $\pm 2.2\,\mu\varepsilon$) had been installed to measure circumferential and axial strains. To minimize the boundary effect, the strain gauges were assembled at Section A and Section B which are 1.5 m from both ends of the pipe. The 8 circumferential gauges were used to measure the pipe crest of the exterior wall strain, and 24 circumferential and axial gauges were used to measure the strain of pipe interior wall corresponding to the crest and the valley; the gauges were laid out as shown in Figure 2.

A data acquisition instrument (DH5921 dynamic stress-strain analysis system) was used to record the measured pipe strains for once per second. The system is designed for dynamic structural performance testing in large-scale engineering testing and product development processes and is capable of accurately measuring parameters such as strain, force, and displacement. The instrument design connects the strain gauge to the acquisition system through the wire. The instrument sensitively collects and amplifies the weak voltage signal, then converts the voltage signal into true strain by the associated program calculation, and then transmits the data to the computer through the Ethernet. The strain readings were zeroed after installation; the tensile strains and compressive strains are reported as positive values and negative values, respectively. The pipe wall strains at the instrumented pipe sections were monitored and recorded after 5-minute load application.

As to the field installation of pipe in this test, the 6 m pipe was installed in two different compaction conditions, in which the backfill in the range of 3.0 m was compacted according to the standard outline by CJJ 143-2010 [33]; in another region, the backfill under the left-haunch was not compacted during installation and was used to simulate the extreme conditions of the backfill poor compaction. The backfill was compacted with a vibratory plate tamper and a plate of 450 mm × 450 mm, with an operating mass of 500 kN. The HDPE pipe was buried and tested under a trench with the length of 6.0 m, the width of 2.2 m, and the depth of 2.4 m, and both ends of the pipe were constrained by inspection wells. The parameters of the backfill sand are profiled in Table 2.

Table 1: Properties of HDPE pipes' geometry and material.

Properties	Value
Nominal diameter (mm)	800
Corrugate length (mm)	100
Corrugate height (mm)	55
Minimum lamination wall thickness (mm)	3.5
Minimum interior wall thickness (mm)	2
Cross-sectional region per unit length (mm^2)	8.7
Moment of inertia per unit length (mm^4)	5,120
Hoop stiffness (kPa)	8

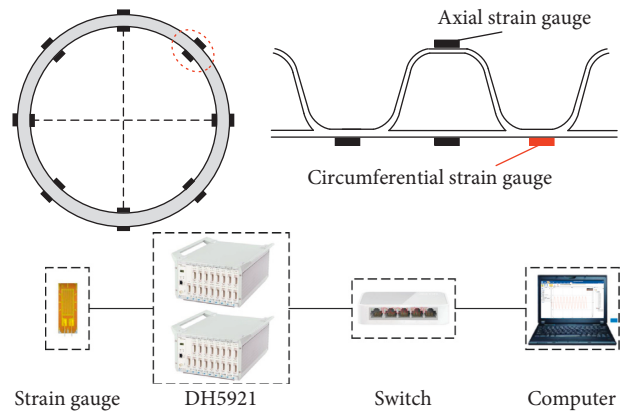

Figure 2: Location of strain gauges and the data acquisition method.

The standard installation process in the 3.0 m region during the field test is plotted as follows. The bottom of the trench had a 200 mm thick bedding layer consisting of the sand with 90% compaction (i.e., Lay 01) overlaying the undisturbed natural soil. The region (i.e., Lay 02) from the bedding to haunch was backfilled with 95% related density to provide strong support for the pipe. From the springline of the pipe to the crown of the pipe, the sand backfill was placed surrounding the pipes in lifts of 100 mm and compacted until 95% compaction before the subsequent lifts were added (i.e., Lay 03). The 0.4 m region of the crown of pipes was divided into two parts (i.e., Lay 04 and Lay 05), and the sand backfill had compactions of 85% and 90%, respectively. In the 1.0 m thick range (i.e., Lay 06) from 0.4 m above the crown of the pipe to the ground, the in-suit soil with 90% compaction was placed. Under the condition of uneven compaction of backfill soil, the soil was not compacted when the left-haunch (i.e., the left side of Lay 02) was backfilled, and the remaining regions were compacted according to the standard requirements. The region of backfill was divided and compacted as shown in Figure 3.

2.2. Field Test of Pipe. In this field test, there was no pavement layer overlying the surface of soil, and the strain of the pipe was much greater than the real deformation of the pipe buried under

Table 2: Basic properties of the field-test soil.

Properties	Value
In-suit soil	
Maximum dry density (kg/m^3)	1549
Water content (%)	12
Liquid limit (%)	25.9
Plastic limit (%)	17.3
Void ratio	42.3
Backfill sand	
Maximum dry density (kg/m^3)	1730
Coarse sand (0.5~3 mm) (%)	35
Medium sand (0.35~0.5 mm) (%)	57
Fine sand (0.25~0.35 mm) (%)	8
Grade	120

the pavement. Therefore, the measured data are only used to be compared with the simulated data, in order to verify the accuracy of the numerical model; however, it cannot be considered as the pipe deformation under the real vehicular load.

Two inspection wells were provided at both ends of the pipeline, and the vehicular load was applied to a heavy truck. Figure 4 shows the tire positions of the two axles of the truck for the pipe. The rear axle of truck was assumed to share 2/3 of the total load and the centre of gravity of the rear axle was exactly above the section with strain gauges. The truck total load was 168 KN and each rear tire applied to the surface was 700 kPa.

3. Finite Element Formulations

3.1. Analytical Model. For the flexible buried pipe, estimate of pipe deflection and strain can be calculated using design equations. A simplified procedure which is suitable for hand calculation is being developed based on design equations for solving the deformation and strain of buried flexible pipes [34]. The deflection caused by the hoop compression and bending is taken into account, and the amount of change in the diameter in the vertical direction is obtained (equation (1)). Then, Watkins et al. used the empirical "shape" factor D_f to represent the peak circumferential bending strain as a function of displacement (equation (2)) [35]. However, as an empirical coefficient, D_f is difficult to generalize the strain distribution of all polyethylene pipes, and for HDPE double-wall corrugated pipes with a special cross-sectional shape, the empirical coefficient D_f is more limited.

$$\frac{\Delta_v}{D} = \left(\frac{q_v}{(EA/R) + 0.57M_s}\right) + \left(\frac{D_l K q_v}{(EI/R^3) + 0.061M_s}\right), \quad (1)$$

$$\varepsilon_b = D_f\left(\frac{c}{R}\right)\left(\frac{\Delta_v}{D}\right), \quad (2)$$

where Δ_v = vertical diameter decrease; D = pipe diameter; q_v = overburden pressure at springline; E = pipe material modulus; R = radius of the centroid of the pipe section; M_s = one dimensional soil modulus; K = bedding coefficient; D_l = deflection lag factor; A = area of the cross section; I = moment of inertia; c = distance to the extreme fiber from the neutral surface within the pipe wall; ε_b = peak circumferential bending strain; and D_f = empirical strain factor relating the bending strain to bending deflection.

3.2. Model of the Soil. According to the parameters of the HDPE pipe profile and soil used in the field test, we establish a three-dimensional finite element model. Attributable to the pipe exterior wall is the corrugate corresponding soil model having a complicated shape in the contact region, and the exterior wall meshes have coincided with the soil meshes to ensure the accuracy and comparability of the simulation result.

Therefore, the meshing of the "corrugated" area of the soil model is very difficult. In order to control the quality of the elements and ensure the accuracy of the model, the elements size of the soil corrugated area should be small enough. This inevitably makes the element number of corrugated soil much larger than the element number of normal straight wall pipes, the size of the model and the computational efficiency are unbearable for ordinary computers. In this paper, the professional meshing software HYPERMESH is used to mesh the corrugated soil model, and under the condition of ensuring the calculation accuracy, the number of elements is subtly reduced, so the number of soil model elements used in this article is only 630,000. In HYPERMESH, the plotted refined numbered elements and the exterior wall shell elements are generated based on the corresponding pipe-soil interface mesh, and the elements of the contact positions between the interior wall and the exterior wall must also coincide. The independent elements of pipe and soil are exported from HYPERMSH and are inducted into ABAQUS for analysis (Figure 5).

The soil model is 3.0 m long, 4.0 m wide, and 3.6 m deep (Figure 6) and is simulated by the Mohr–Coulomb constitutive model. The soil elements are the eight-node reduced-integration element (C3D8R) and the hourglass is well enhanced. The compaction of the backfill is illustrated in Figure 6, and the backfill parameters for numerical simulation can be seen in Table 3. The mechanical parameters of loose backill such as elastic modulus and Poisson's ratio and cohesion are different from the compacted backill. For the flexible pipe, the elastic modulus of soil (i.e., the stiffness of soil) directly affected the interaction between the pipe and soil; if the backfill is loose, the elastic modulus of backfill is reducted, the soil-pipe interaction is weakened, and the soil load assumed by the pipe is increased. In this paper, the backfill looseness is manifested by reducing its elastic modulus.

According to the Structure Design Code for Pipelines of Water Supply and Waste Engineering (GB 50332-2002), the relationship between soil compaction and elastic modulus is presented; in the next part of numerical model validation, the elastic modulus of loose backfill is designed as 3 MPa. The bottom plane of the soil is fully constrained, and horizontal displacements of the four vertical planes are not allowed.

3.3. Model of the Pipe. The elastic model and the eight-node reduced-integration shell element (S8R) are used to simulate the pipe of the initial interior diameter of 0.8 m and the length of 3.0 m (Figure 7). The pipe is considered as an elastic material because of its linear elasticity in short-term load; the material parameters of HDPE pipe presented in Table 4 are

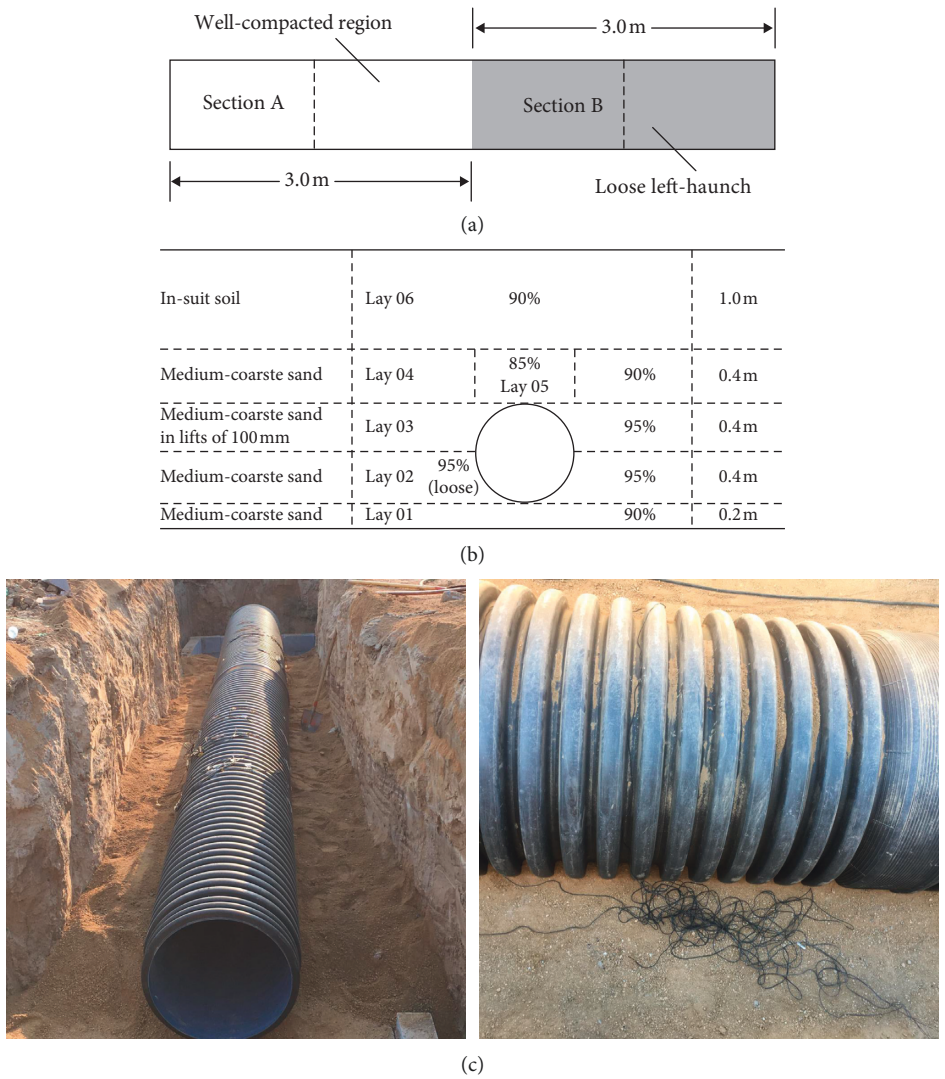

Figure 3: (a) Location of the measuring sections; (b) material and compaction degree of the backfill by specification; (c) field installation.

suggested by the Specification of Technical Specification for Buried Plastic Pipeline of Sewer Engineering [33].

3.4. Model of the Vehicular Loads. The structure model simulated the foundation and does not consider about the pavement and the subgrade; the vertical load σ_z applied to the foundation is consisted of σ_{z1} and σ_{z2}; σ_{z1} is the vehicular load and σ_{z2} is caused by the pavement structure and subgrade.

In the 1960s, the fourth power theory was proposed by the American Association of Interstate Highway Workers (AASHO): static axle load is more suitable for simulating traffic load with low speed and light axle load [36]. In the "Specification for Design of Highway Asphalt Pavement," the truck whose rear wheel is a uniaxial-dual-wheel is specified as a standard vehicle and 100 kN as a standard axle load. In this paper, the single-circle load is adopted to simulate the dual-wheel group of the rear wheel of heavy vehicles, the diameter of the circle load (D) is 300 mm, and the dual spacing of vehicle wheels is 1.8 m and the standard load (p) is 0.7 MPa. The vehicular load acting on the road surface is dispersed during the downward transfer. The expansion angle of subgrade pressure is related to the load width and the elastic modulus of the underlying layer. According to the Code for design of building foundation, the expansion angle of each pavement layer and the diameter after dispersion are as shown in Figure 8. When dispersed to the surface of the foundation, the circular load has a diameter of 1.8 m, and the 3.5 m wide lane is filled with uniform load. The vehicular in the city is continuous and slow, so the traffic load can be simplified to a uniform static load applied across the entire foundation. The vertical stress σ_{z1} caused by the vehicular load is related to the thickness of subgrade and the expansion angle of subgrade pressure (equation (3)) The vertical stress σ_{z2} of the foundation surface caused by the pavement structure and subgrade is seen in equation (4):

$$\sigma_{z1} = \frac{D^2 p}{(D + 2z\tan(\theta))^2}, \tag{3}$$

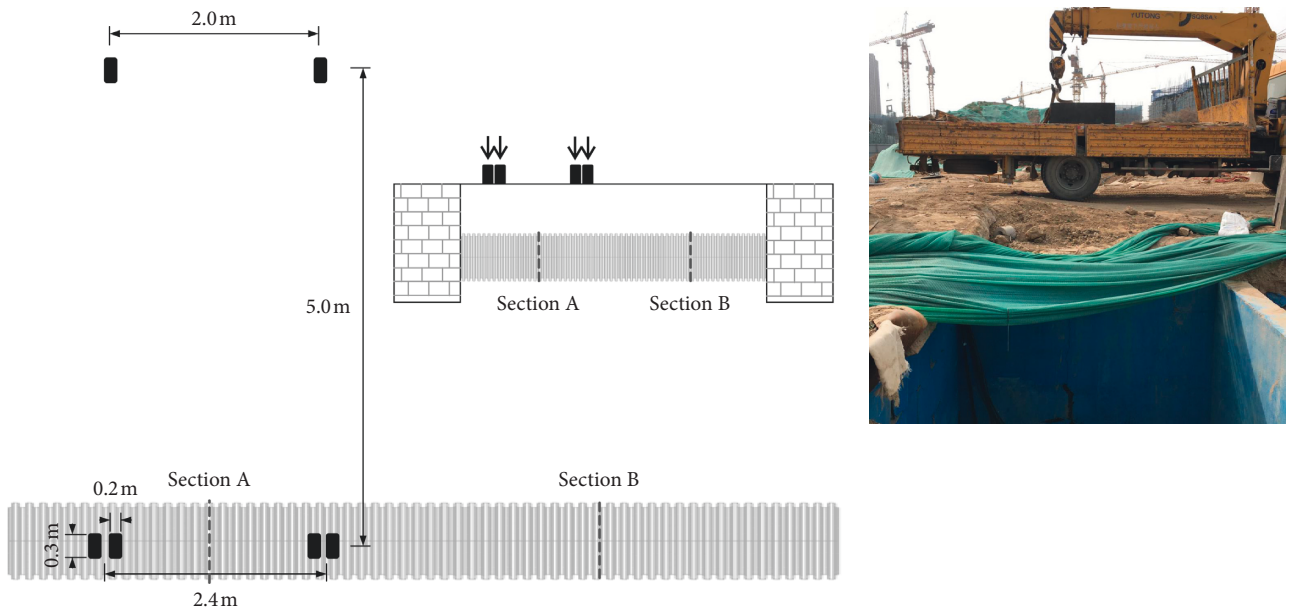

Figure 4: (a) Location and parameters of wheel loads; (b) field test.

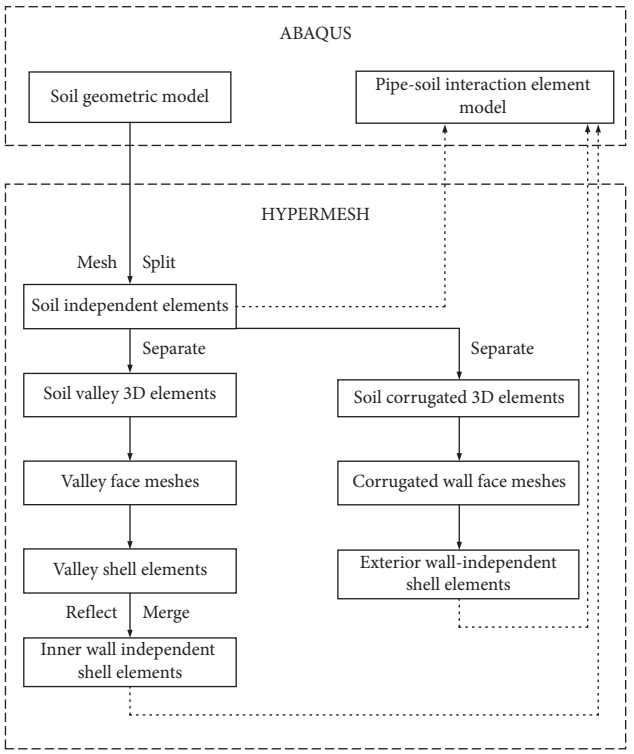

(a)

Figure 5: Continued.

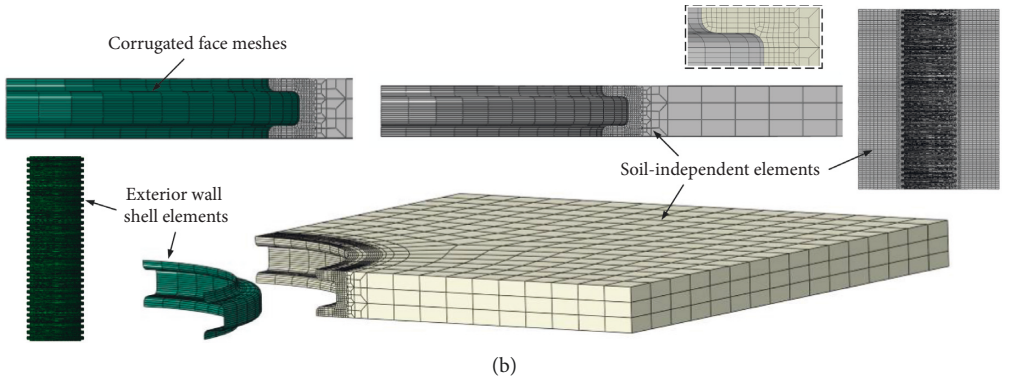

Figure 5: (a) Mesh generation scheme using HYPEMESH; (b) elements of soil and pipes' exterior walls.

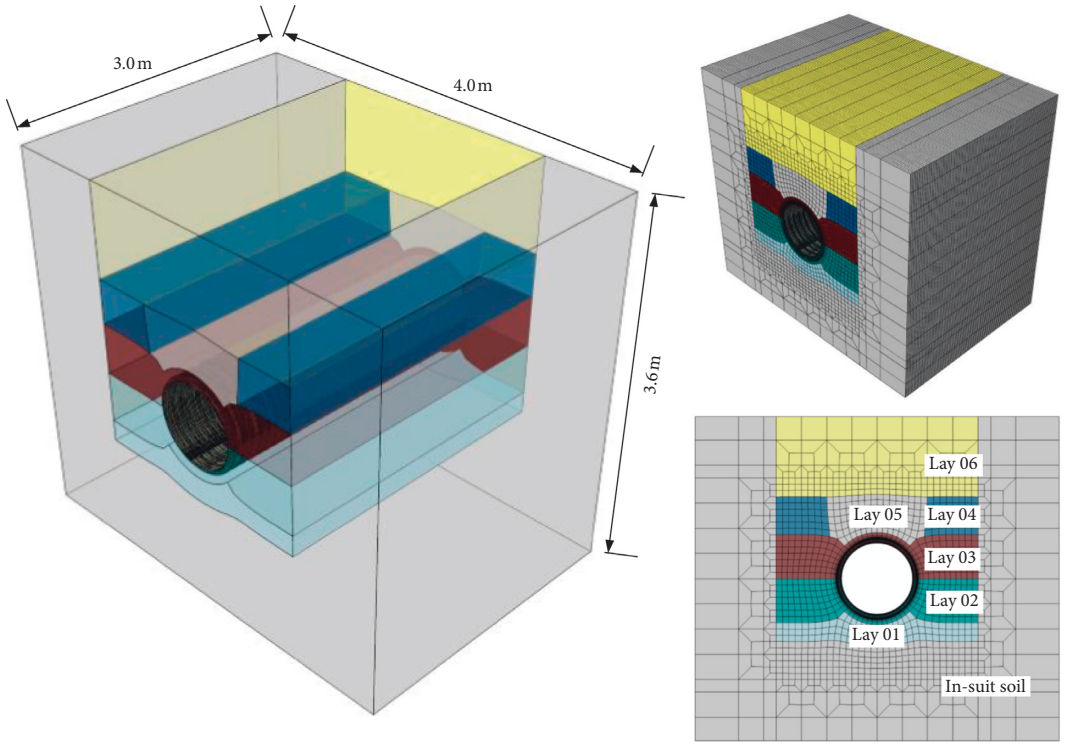

Figure 6: Three-dimensional calculation mode.

Table 3: Properties of soil used for numerical simulation.

Properties	Lay 01	Lay 02	Lay 03	Lay 04	Lay 05	Lay 06	In-suit soil
Dry density (kg/m^3)	2020	1670	1670	2020	2000	1800	1850
Related density (%)	90	95	95	90	85	90	
Elastic modulus (MPa)	10	15	15	7	9	9	30
Poisson's ratio	0.30	0.26	0.26	0.23	0.30	0.32	0.35
Cohesion (kPa)	0.50	0.25	0.25	0.30	0.35	0.40	0.40
Friction angle (°)	35	31	25	28	30	27	30

where D = diameter of circular load, p = magnitude of tire pressure, z = distance from the base bottom to the top of the foundation, and θ = expansion angle of subgrade pressure.

$$\sigma_{z2} = \gamma_1 h_1 + \gamma_2 h_2 + \gamma_3 h_3, \quad (4)$$

where γ_1 = severe of surface course, h_1 = thickness of surface course, γ_2 = severe of base course, h_2 = thickness of base

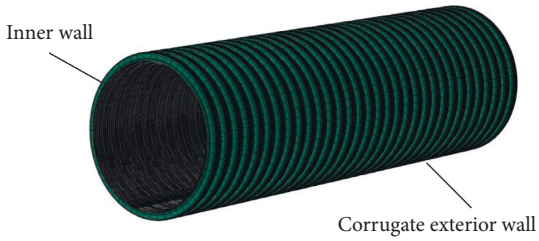

Figure 7: Elements of double-wall corrugated pipe.

Table 4: Idealized thickness of pipe walls for numerical simulation.

Properties	HDPE corrugated pipes
Modulus of elasticity (MPa)	800
Density	950
Poisson's ratio	0.4
Idealized exterior wall thickness (mm)	3
Idealized interior wall thickness (mm)	2

course, γ_3 = severe of subgrade, and h_3 = thickness of subgrade.

By equations (1) and (4), the vertical stress σ_z of the applied load on the surface foundation soil is 50 kPa. Therefore, the 40 kPa and 3.28 m × 3.08 m static load acting on the foundation soil is employed by simulating the vehicular loads acting on the pipe in this paper.

4. Verification of Numerical Models

Corresponding numerical models are established according to the implementation of the full-test; the vehicular load is applied according to the position of the tire in the test and the load size is 0.7 MPa.

It can be seen from Figure 9 that the calculated results of circumferential strain are basically consistent with the measurement results of the full-scale test in distribution trends and values. The calculated value of the axial strain and the measured value of the interior wall are greatly different, which may be because that the strain gauge used in the test is long and the axial strain record in the test is not accurate enough. It indicated that the simulated parameter series is fully validated by the full-scale test, thus making it reasonable to believe that the structure models in this paper are reasonable and reliable.

For pipe with the uniform backfill, the maximum compression value of the pipe can be represented by the circumferential strain on the valley or the interior wall at the springline [27]. The circumferential strain distribution of the liner is similar with that of the valley, except that the liner is of greater magnitude. The circumference strain firstly increases and then decreases; the maximum circumferential strain occurs at the springlines and the strain at the crown is less than that at the invert. The maximum circumferential strain of the liner wall is less than the minimum valley circumference strain, and the circumferential strains varied greatly in small regions. This indicates that the local buckling in the profile and the interior wall springlines is more like to be damaged [37]. The distribution of the crest circumferential strain is complex. The strain decreases from the crown to the shoulder and then increases from the shoulder to the springline, and then decreases from the springline to the invert. The minimum strain and the maximum strain appear on the shoulder and the springline, respectively. The valley axial strain is the tensile strain, the axial strain is much less than the circumferential strain, and the influence on pipe is not considered, for the strain value is too small.

The result of the circumferential strain distribution is slightly different from that reported in the literature; this may be caused by different compaction methods and backfill materials during pipe installation. The detailed report of the measured circumferential strains can be found in the study by Brachman [19]. Brachman pointed out in the paper that the maximum circumferential strain of the valley appears at the springline, and the valley circumferential strain at the crown is great than that at the invert; the crest circumferential strain is greatest at the springline; and the strain at the invert is greater than that at the crown. The axial crest strain is tensile except for that at the springline.

Figure 10 plots out the distribution of pipe strains when the backfill under the left-haunch is loose, and the measured strain deviates greatly from the calculated strain, perhaps due to the location of the strain gauge and the effect of nonuniform backfill support to pipe. Nevertheless, within the allowable range of error, the distribution trends of the general agreement between the measured strain and the calculated strain are obtained from the finite element model. Therefore, it is considered that the three-dimensional finite element model can provide reliable calculated analysis results for studying the mechanical response of the pipe in the case of nonuniform backfill, and setting the modulus of loose backfill to 3 MPa in numerical simulation is considered trustiness.

Based on the three-dimensional finite element model, effect of loose backfill of different regions on the pipe strain and deformation are studied under the vehicular load in the next part. The distribution of circumferential strain discussions is highlighted and considered to be a more sensitive indicator of deformation, and the difference between liner circumferential strain and valley circumferential strain is regarded as an indicator of the possibility of local buckling.

5. Effect of Loose Backfill

If the compaction of the backfill is asymmetrical, the pipe is eccentrically compressed. Under the long-term load, the eccentric compression of the pipe is more likely to cause the failure of the pipe. Since the specification requires attention to the compaction of backfill under the haunch of the pipe, in this part, the most severe conditions considered may exceed typical design conditions. Some compaction conditions are designed on the left and right regions of the backfill compaction which are asymmetrical; the strain distribution and deformation of the pipe are studied under the vehicular load. The possibility of local buckling is indicated through the difference between circumferential strain of the liner and circumferential strain of the valley.

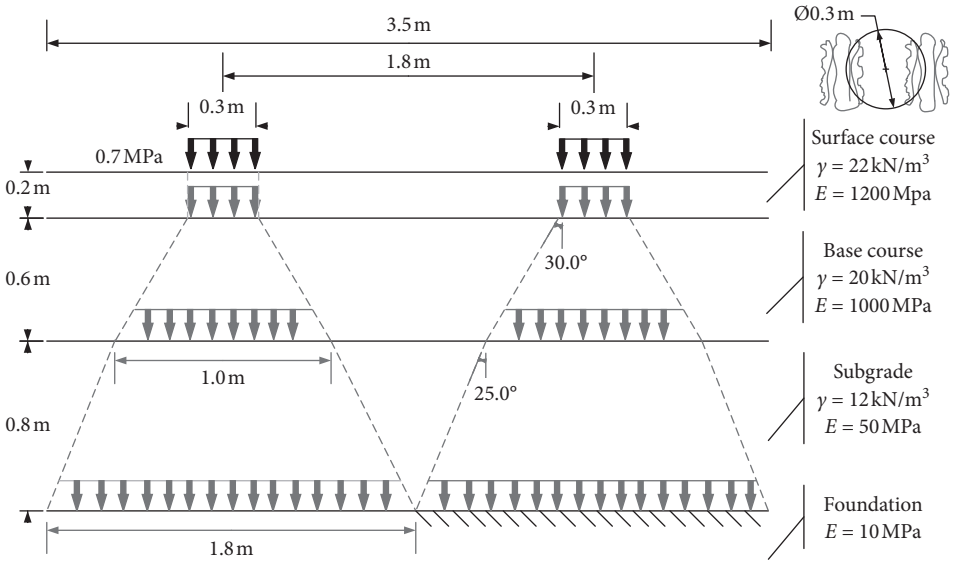

Figure 8: Traffic load dispersion and parameters of urban road.

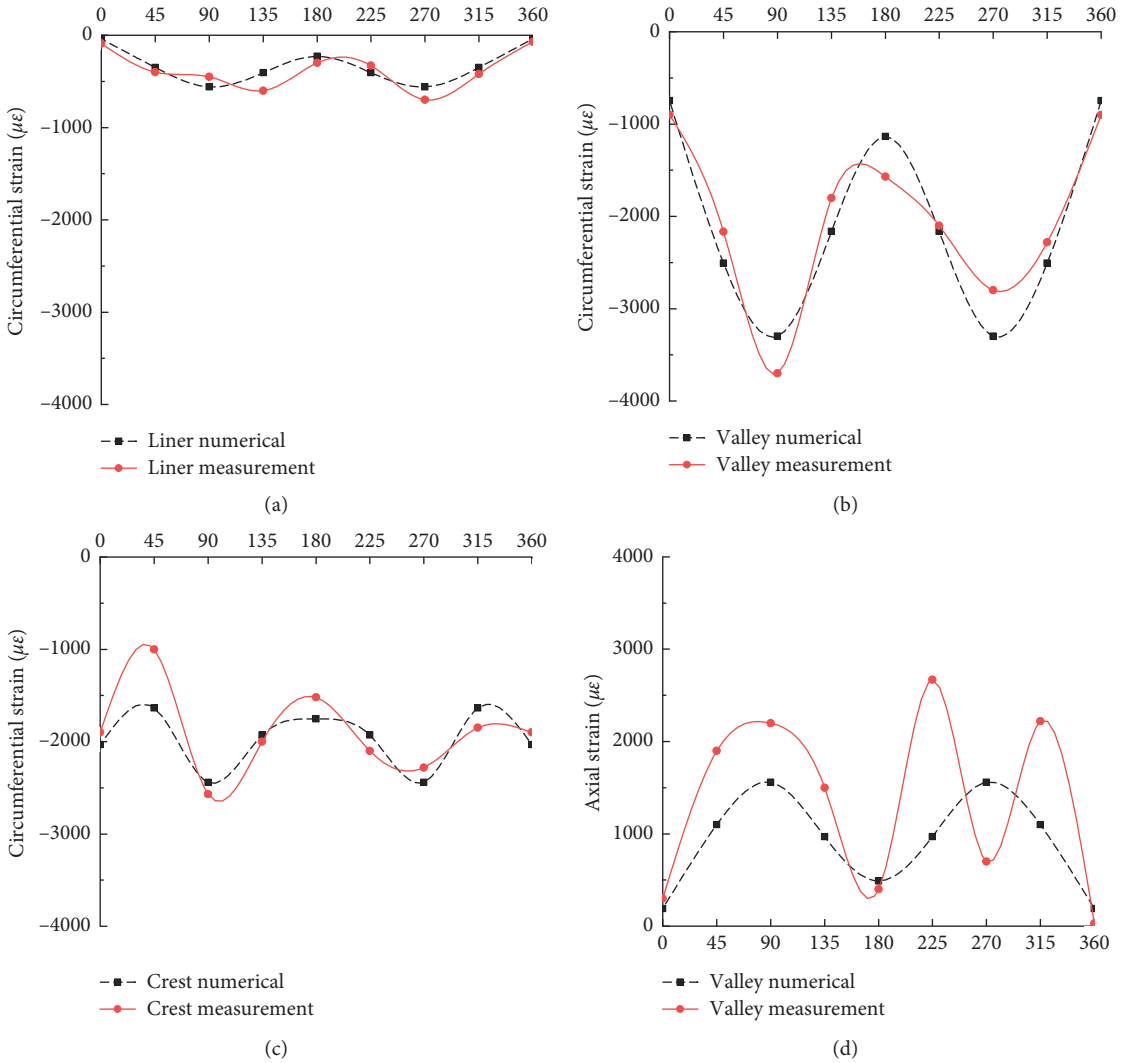

Figure 9: Comparison of measurements and calculation of pipe strains in the well-compacted backfill: (a) liner circumferential strain; (b) valley circumferential strain; (c) crest circumferential strain; (d) valley axial strain.

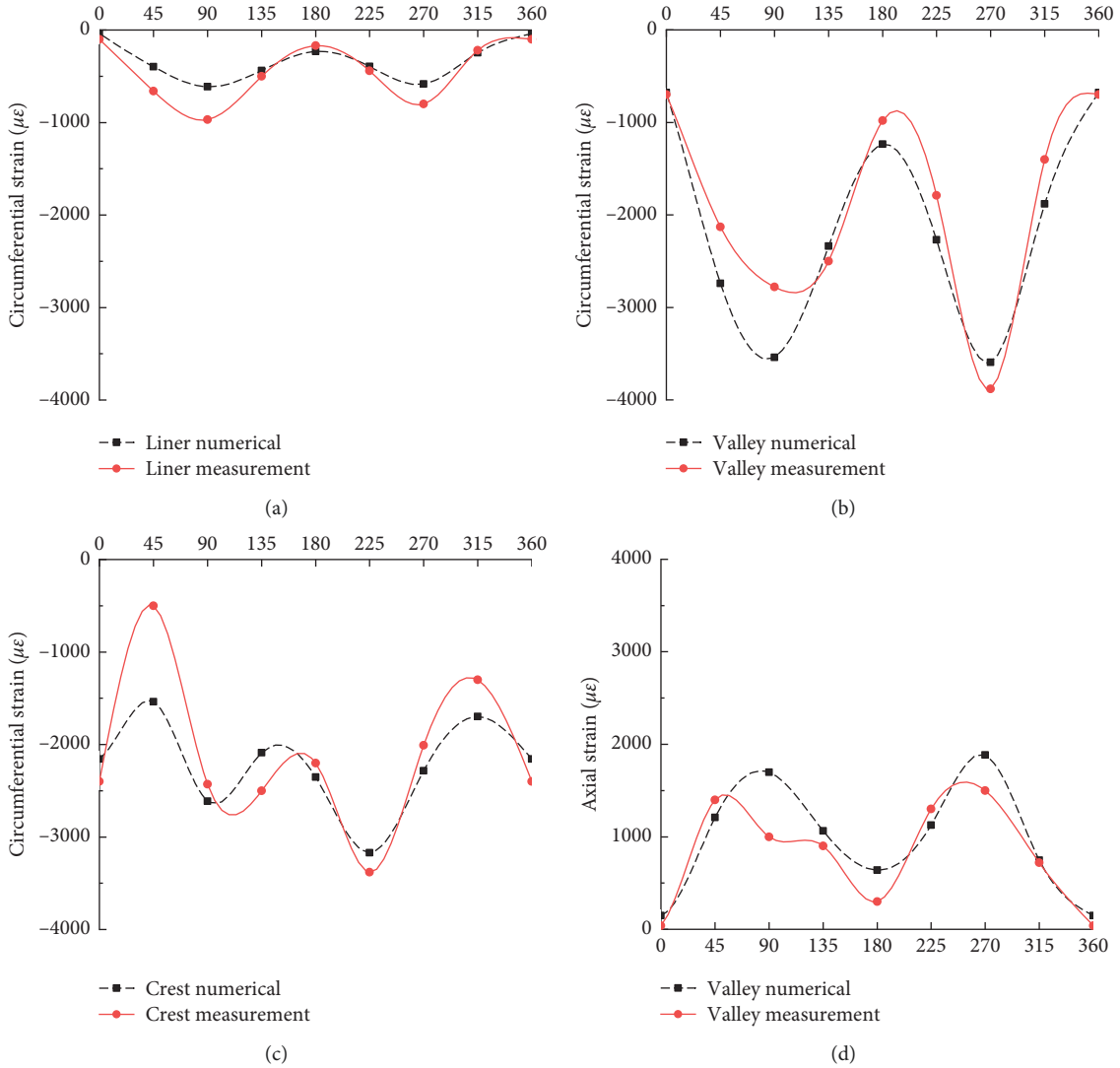

Figure 10: Comparison of measurements and calculation of pipe strains in the poor haunch backfill: (a) liner circumferential strain; (b) valley circumferential strain; (c) crest circumferential strain; (d) valley axial strain.

This part uses a static load of 50 kPa and 3.28 m × 3.08 m to act on the foundation soil.

In Figure 11, LE represents the true strain along the direction of the second axis in ABAQUS, and the local cylindrical coordinates of the pipe are established in the model, so LE22 indicates the circumferential true strain of the pipe. In Figure 12, "Standard" refers to the strain of the pipe under the vehicular load when the backfill is compacted according to the specification. "L01" refers to the strain of the pipe under the vehicular load when the backfill of Lay 01 left region is loose.

5.1. Effect of Loose Backfill of the Single Side. The distribution of circumference strain and displacement of pipe when the left base is softer (i.e., the backfill of left Lay 01 was loose) is plotted in Figures 11 and 12. The circumferential strain of the interior wall increases in the small region (i.e., 180°–225°) and then decreases immediately (i.e., 225°–360°). The maximum circumferential strain of the interior wall appears at the right-springline, and that point is defined as the most dangerous point. The strains of the liner and the valley decrease by 13% and 15%, respectively, at the left-springline. Although the pipe is not in direct contact with the loose backfill, the displacement of the pipe still increases at the lower left of the pipe due to the softness of the foundation. The exterior wall of the pipe is adversely affected only near the invert, and the crest strain on the left side of the pipe is reduced. This shows that the proper reduction of the stiffness of the base of the pipe may reduce the deformation of the pipe.

As plotted in Figures 13 and 14, it is attributed to the low stiffness of the backfill under the left-haunch, which led to the result that the circumferential strain of the interior wall is significantly greater than the standard strain from the invert to the left-springline and decreases from the left-springline to the crown. The maximum strain is near the boundary of the loose backfill and compaction backfill; the maximum strain of the valley and the liner increases by 28% and 34%,

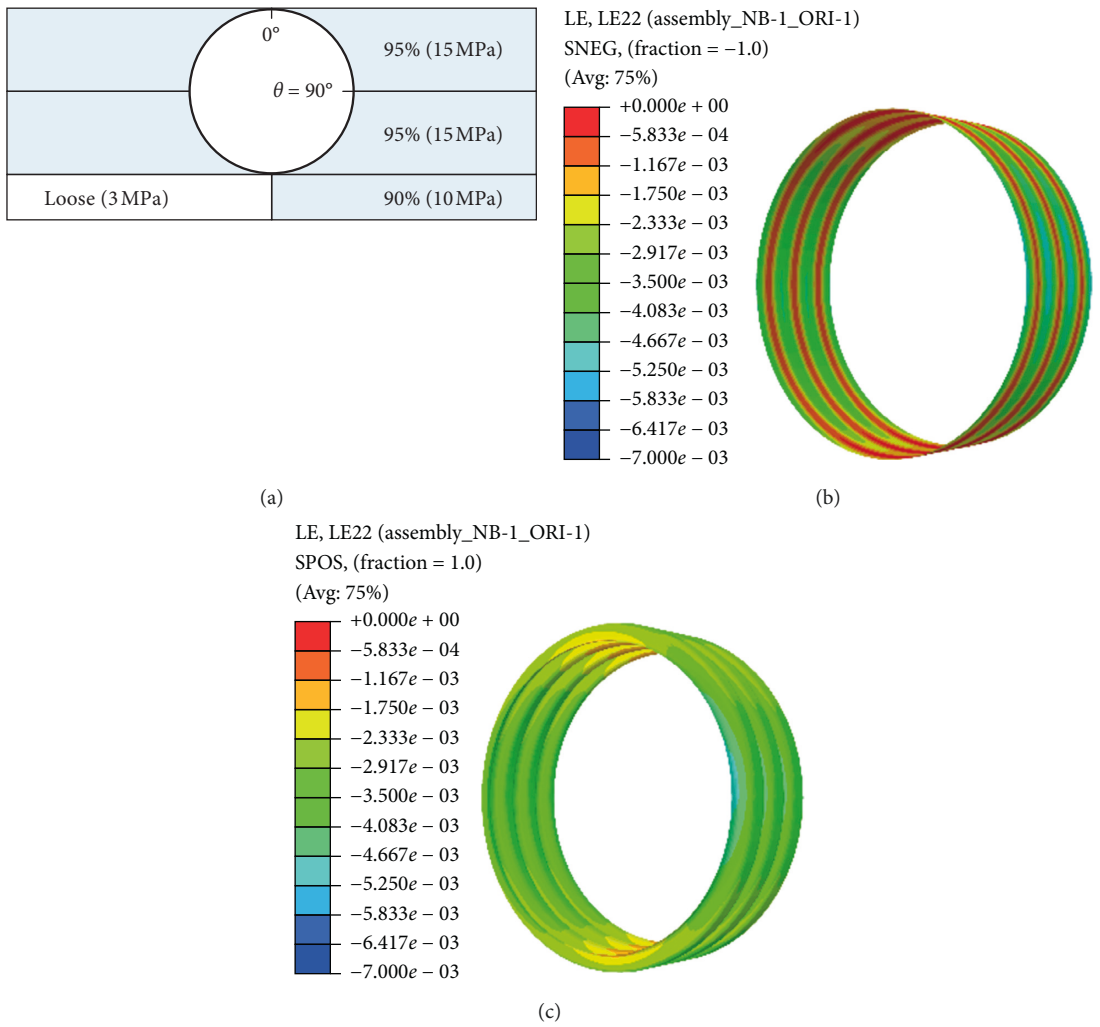

Figure 11: (a) Location of loose backfill; the circumference strain nephogram of the (b) interior wall and (c) exterior wall when the left side of Lay 01 was loose.

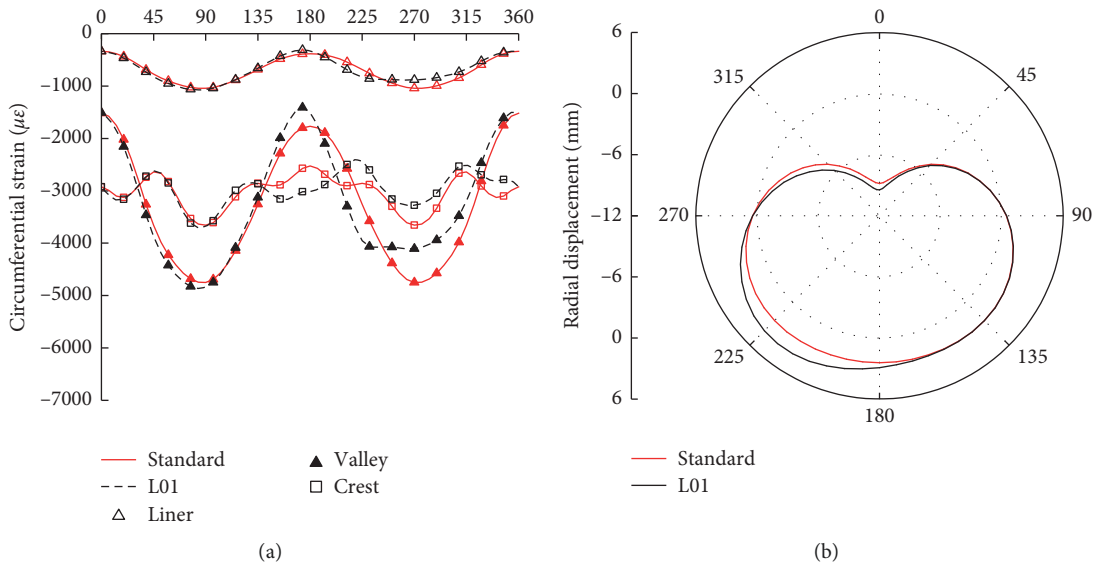

Figure 12: Distribution of (a) circumferential strain and (b) radial displacement when the left side of Lay 01 was loose.

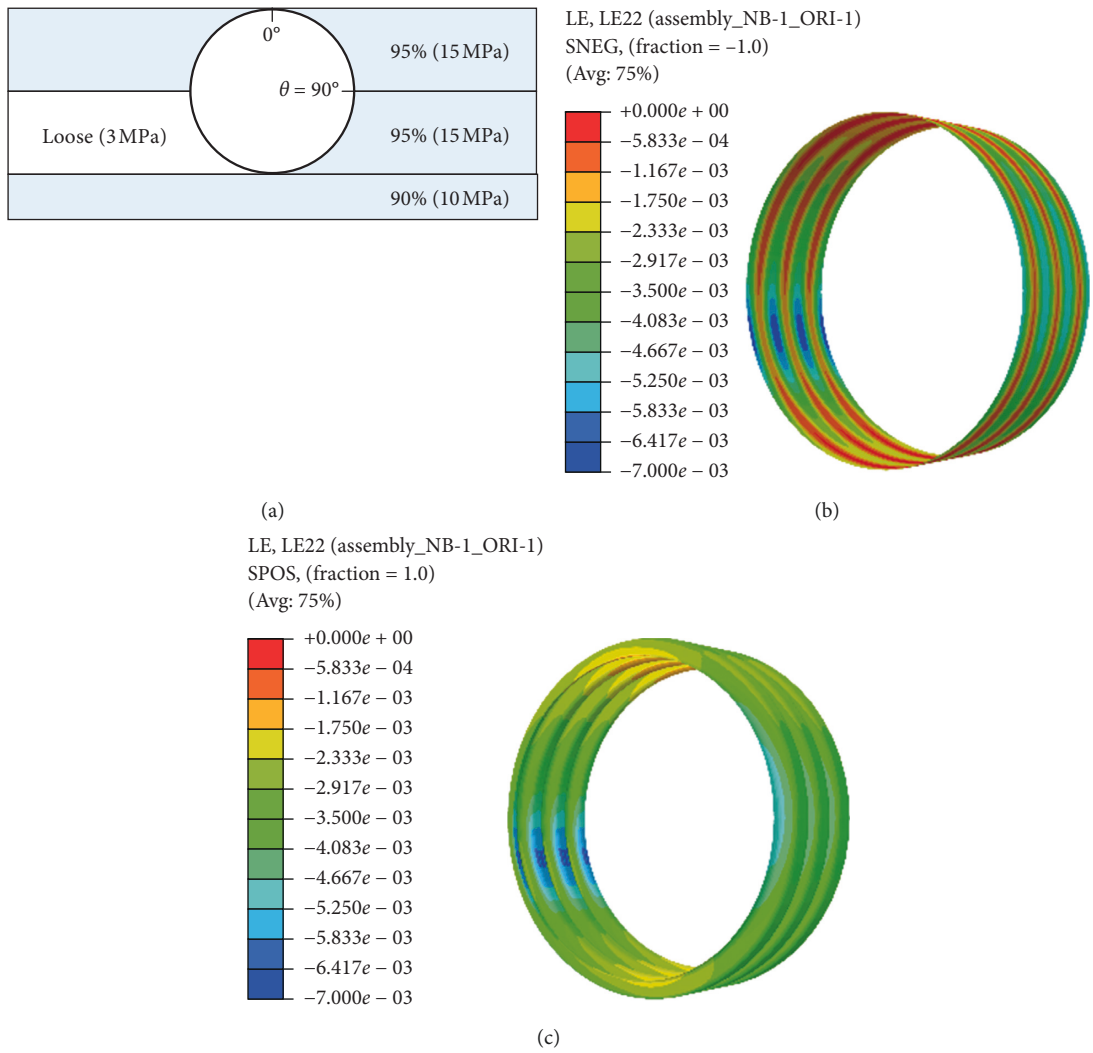

Figure 13: (a) Location of loose backfill; the circumference strain nephogram of the (b) interior wall and (c) exterior wall when the left side of Lay 02 was loose.

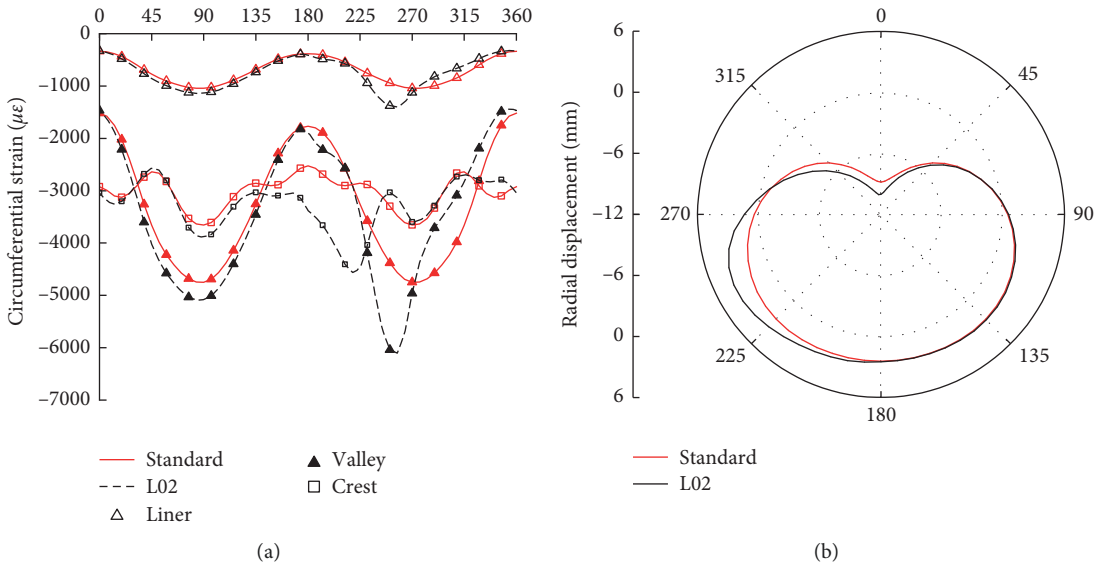

Figure 14: Distribution of (a) circumferential strain and (b) radial displacement when the left side of Lay 02 was loose.

respectively. The maximum of the difference between the valley and liner strains increases by 27%. The softer haunch has an effect on the exterior wall of pipes, which extended from the loose backfill region to the compacted backfill region. The maximum crest circumferential strain increases by 25% (the position moved from the springline to the middle of haunch). The left-haunch of the pipe became the most dangerous position, where local buckling and failure of the exterior wall occurred. At the same time, the radial displacement also varied mostly in this region. The radial displacement of the pipe region constrained by a well-compacted backfill is unchanged, while the displacement of the remaining region increases due to the weakening of the support. The "inverted shape" deformation is characterized by the flattening at the inverted and the protruding haunch [38], and when the soil under the waist is poor and the soil above it was of good quality, the shape of the inverted heart will occur [39]. The description in this part is the same with the conclusion put forward by Dhar et al.; the poor haunch soil led to the strain redistribution around the pipe circumference; strain concentrations occurs at the haunch [2].

For the pipe buried in soil where the backfill of Lay 03 left region in loose, the distributions of strains are shown in Figures 15 and 16. Circumferential strains on the valley and the liner are greater than standard strains on the region from the left-springline to the left-shoulder and are smaller than standard strain on the region from the invert to the left-springline. Maximum valley strain and liner strain increase by 26% and 33%, respectively. Difference between valley strain and liner strain increases by 27% at the right-shoulder. The crest strain of almost the entire pipe increased, and then the position of the maximum crest circumference moves from the springline toward the left shoulder in this case. As the constraint of loose soil on pipeline is weakened, the displacement of the pipe increases near the left-springline and the crown and decreases near the left shoulder (i.e., 290°–315°), while the remaining areas remain unchanged.

Distributions of circumferential strain on the pipe when the Lay 01 and Lay 02 left regions are loose are plotted in Figures 17 and 18. The liner and the valley circumferential strains increase in the region from the invert to the springline (i.e., 180°–270°) and decrease in the region from the springline to the crown (i.e., 270°–0°). The number result shows that the maximum circumferential strain of the liner and the valley increases by 16% and 13%, respectively, near the left-springline; the difference between them increases by 12%, and the part where the local buckling is most likely to occur is also here. The most affected region of the crest circumferential strain is near the invert, and the maximum moves from the springline to the invert, the increasing by 5% arose from the nonuniformity of backfill near invert. However, the crest circumferential strain from the left-haunch extended to the crown decreases. The greater axial displacements at the left side of the pipe prove that the low stiffness backfill region under the springline restricted to the pipe is weak.

Although the loose region of the pipe is larger in this case, the circumferential strain increment caused by the loose backfill became smaller; the influence of the loose backfill on the maximum strain of the pipe is not simply positively related to the size of the loose region.

Figures 19 and 20 show that the strain on the interior wall of the pipe is most affected at above half region of pipe (i.e., 270°–90°) when the left sides of Lay 01 and Lay 03 are loose. The strain increases on the region and reaches the maximum on the left-springline. The maximum of valley and liner increases by 28% and 23%, respectively, and the difference between two strain increases by 21%. The crest circumferential strain fluctuated greatly at the crown, and the maximum of the strain moves from the springline to the crown and increases by 20%. The amount of displacement change is small, mainly reflected in the increase in the crown and the left-haunch region.

When the backfills on the left sides of the Lay 02 and Lay 03 were loose, the structural field determined the deformation and the strain of the pipe (Figures 21 and 22). When the right side of the pipe is supported by the well-compacted backfill, the circumferential strains of interior wall increase. In the left side of the pipe in contact with the loose backfill, the circumferential strains of interior wall increase only in the small region near the springline, and the strain of the rest is reduced. The magnitudes of two peak values at springline are not much different. The maximum strain of the liner and the valley increases by 22% and 14%, respectively, the difference increases by 13%. Near the crown, the crest circumferential strain increases and it is more obvious in the left side. Another region where the crest circumferential strain increased is from the left-haunch to the right-haunch; near the left-haunch, the maximum value appears and increases by 15%. Also, the loose backfill on the left side caused the increase of the axial displacement on the left side of the pipe to increase.

It is assumed that in extreme cases, the backfill on the left side of the pipe is loose, and the strain and displacement of the pipe are shown in Figures 23 and 24. The circumferential strain of valley and liner increase on the springlines and the strain on the right-springline increase more and reach the maximum value, although the right side of the pipe is surrounded by well-compacted backfill. The valley circumferential strain maximum increases by 17% and the liner circumferential strain maximum increases by 24%, the difference which can be used to indicate the possibility of local buckling increased by 14%. The crest circumferential strain distribution law is completely changed and the maximum value appears near the crown, which is increased by 15%. The crest circumferential strain in most areas near the invert increases, and the most vulnerable location of the exterior wall appears at the crown and invert. Under the combined action of the upper soil extrusion and weakening of the surrounding backfill, the radial displacement of the pipe is obviously enlarged in the loose area.

5.2. Effect of Loose Backfill of Both Sides. The circumferential strain distribution and deflection are complex when the combined action of the left side of Lay 01 and right side of Lay 02 is loose (Figures 25 and 26). It can be found that the circumferential strain of the interior wall decreased or

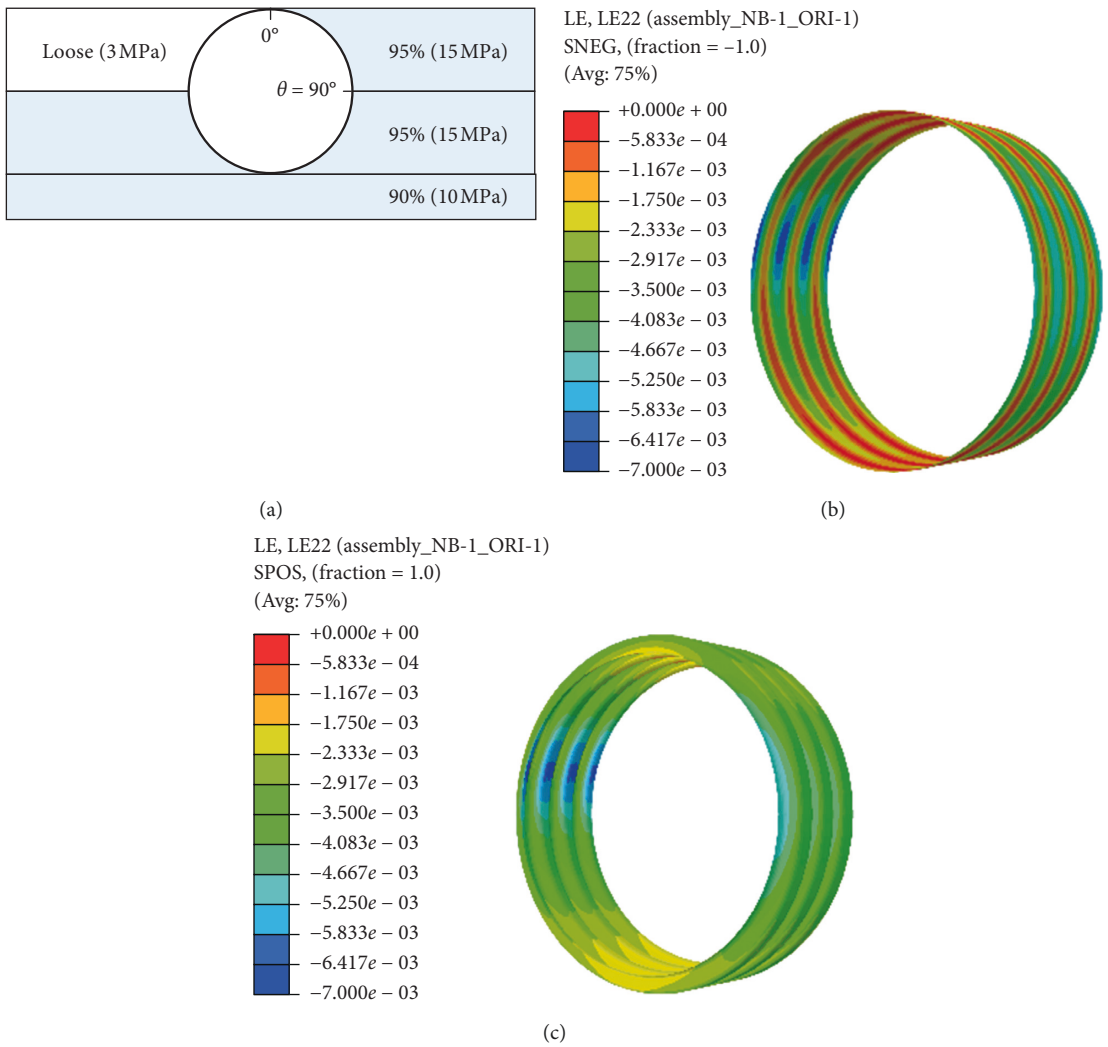

Figure 15: (a) Location of loose backfill; the circumference strain nephogram of the (b) interior wall and (c) exterior wall when the left side of Lay 03 was loose.

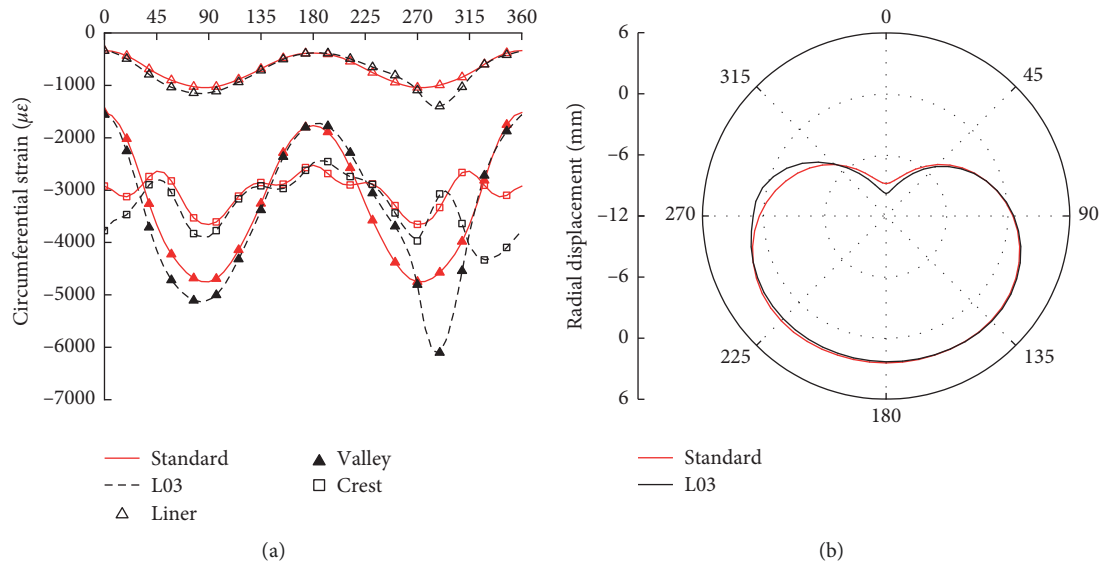

Figure 16: Distribution of (a) circumferential strain and (b) radial displacement when the left side of Lay 03 was loose.

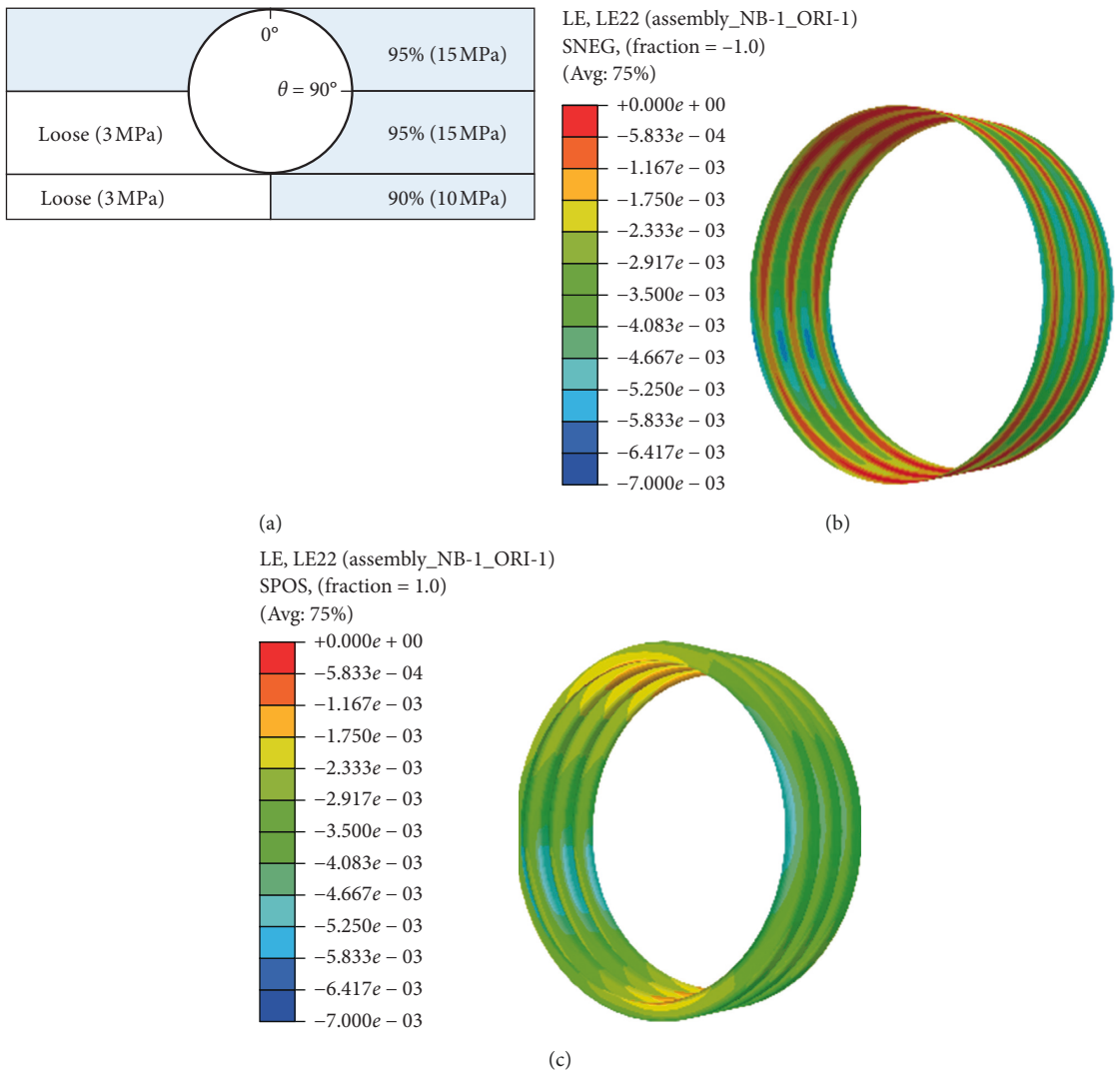

Figure 17: (a) Location of loose backfill; the circumference strain nephogram of the (b) interior wall and (c) exterior wall when the left sides of Lay 01 and Lay 02 were loose.

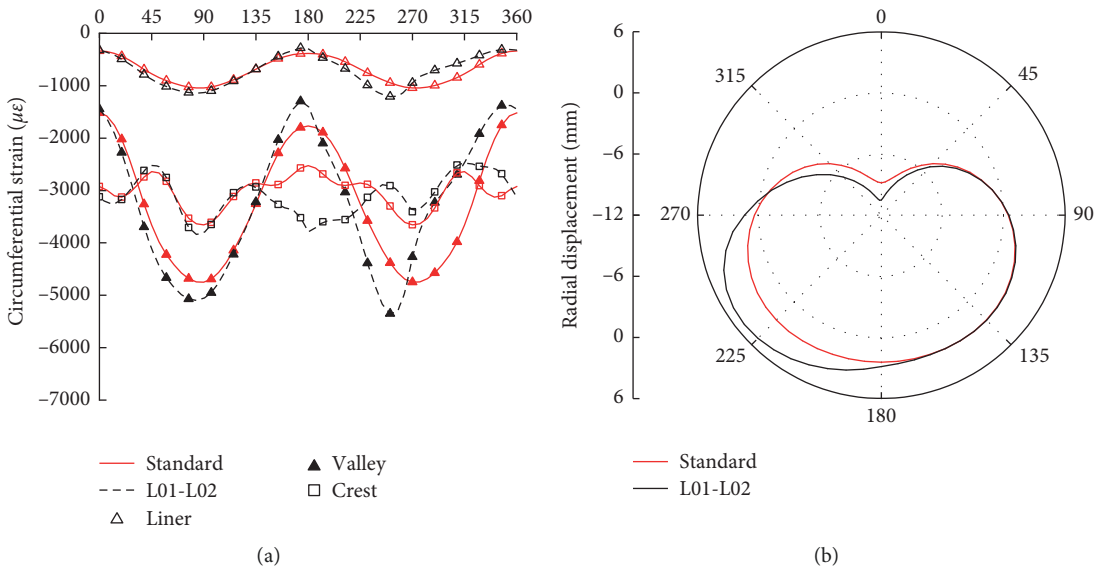

Figure 18: Distribution of (a) circumferential strain and (b) radial displacement when the left sides of Lay 01 and Lay 02 were loose.

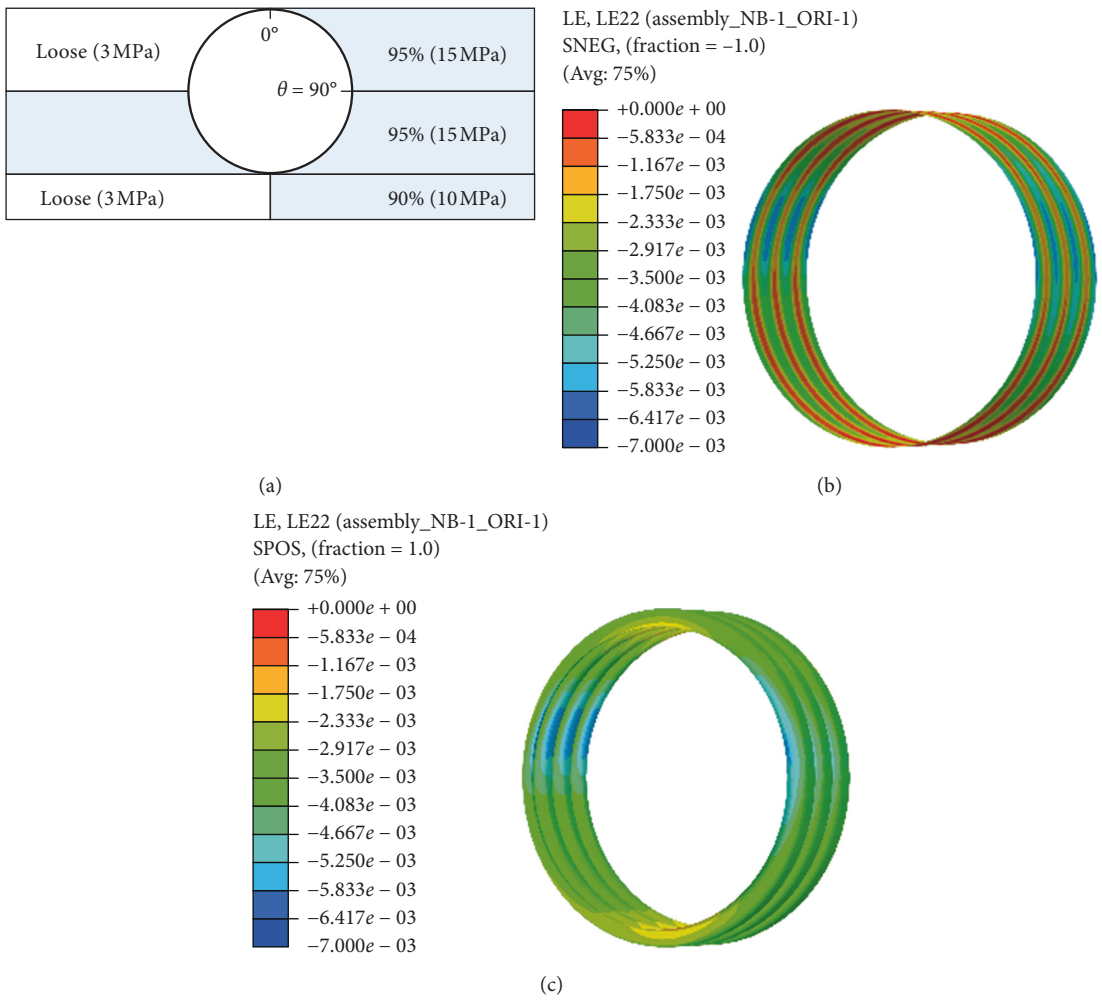

Figure 19: (a) Location of loose backfill; the circumference strain nephogram of the (b) interior wall and (c) exterior wall when the left sides of Lay 01 and Lay 03 were loose.

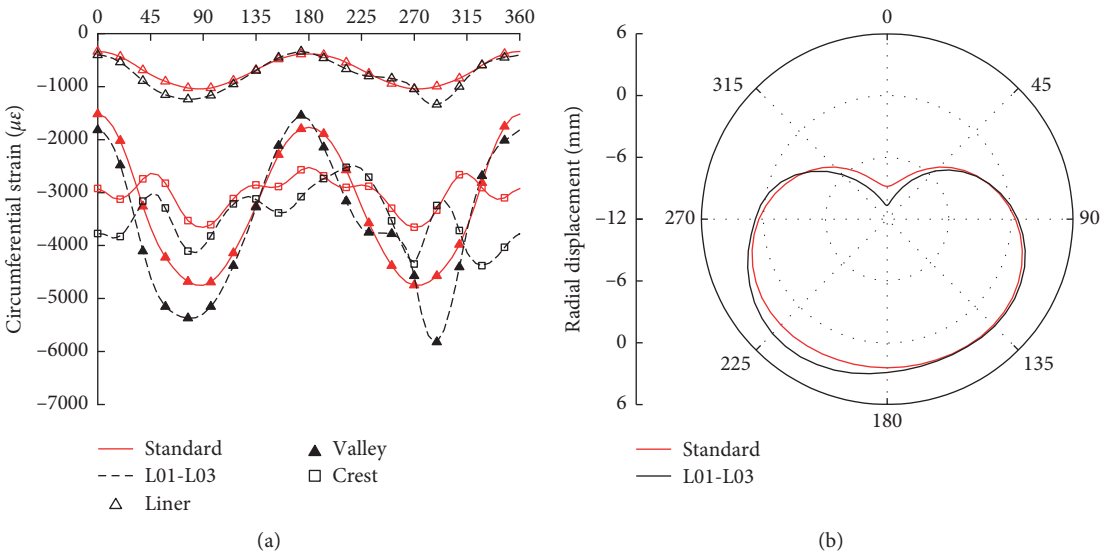

Figure 20: Distribution of (a) circumferential strain and (b) radial displacement when the left sides of Lay 01 and Lay 03 were loose.

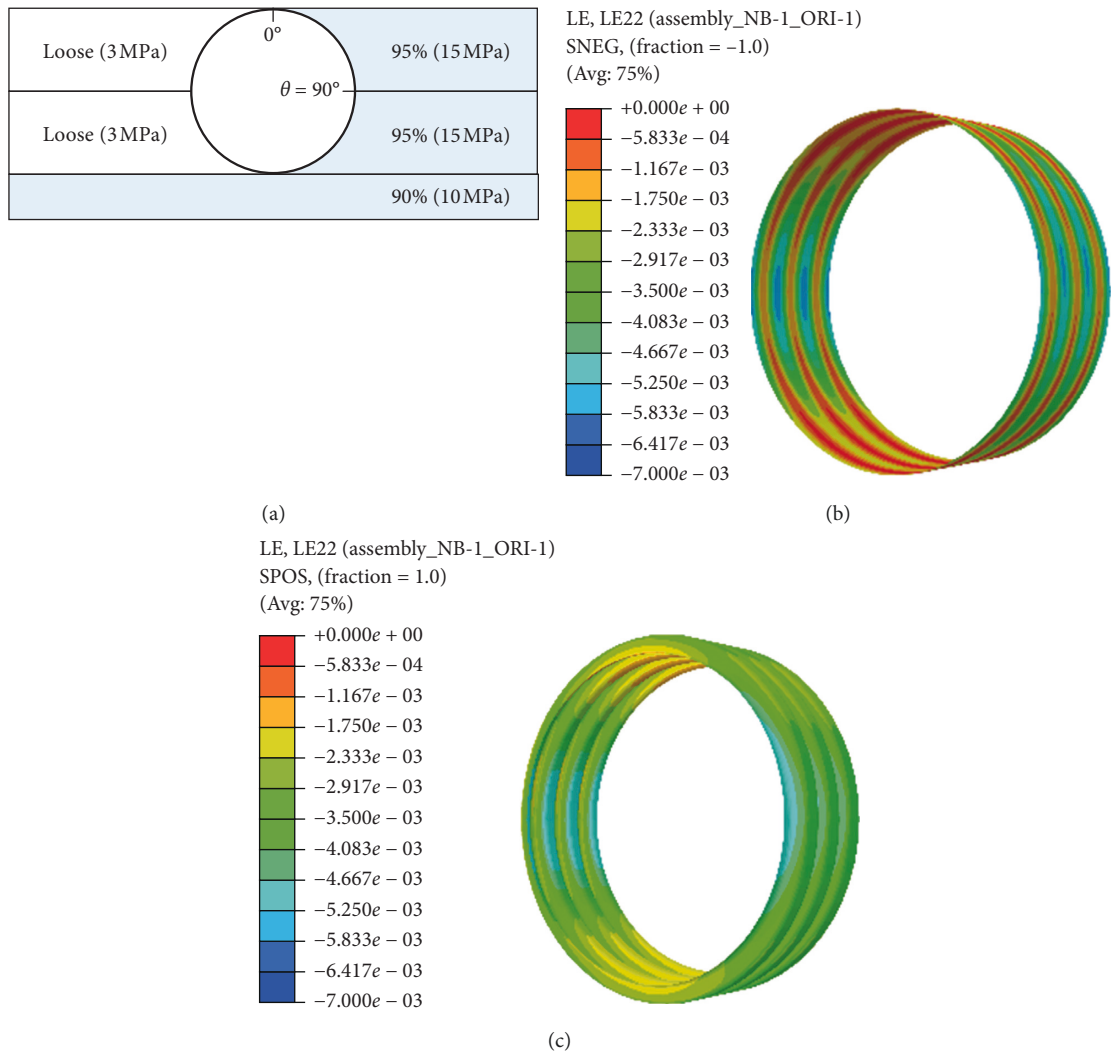

Figure 21: (a) Location of loose backfill; the circumference strain nephogram of the (b) interior wall and (c) exterior wall when the left sides of Lay 02 and Lay 03 were loose.

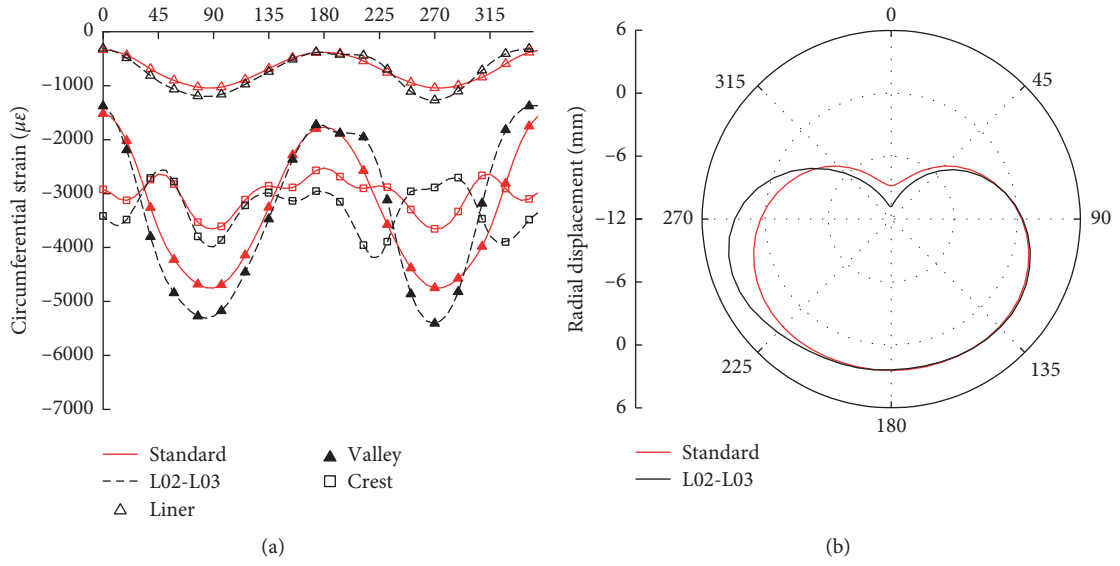

Figure 22: Distribution of (a) circumferential strain and (b) radial displacement when the left sides of Lay 02 and Lay 03 were loose.

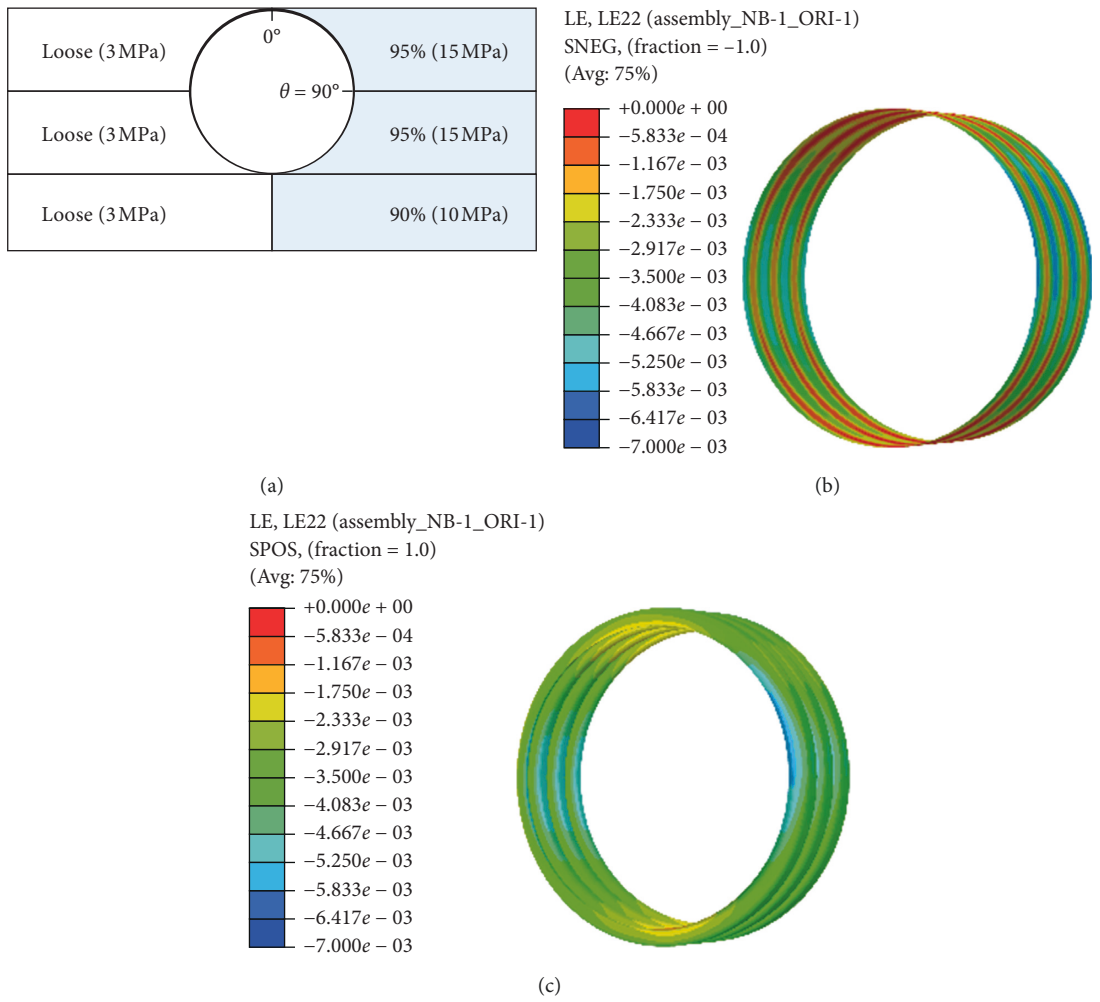

Figure 23: (a) Location of loose backfill; the circumference strain nephogram of the (b) interior wall and (c) exterior wall when the left sides of Lay 01, Lay 02 and Lay 03 were loose.

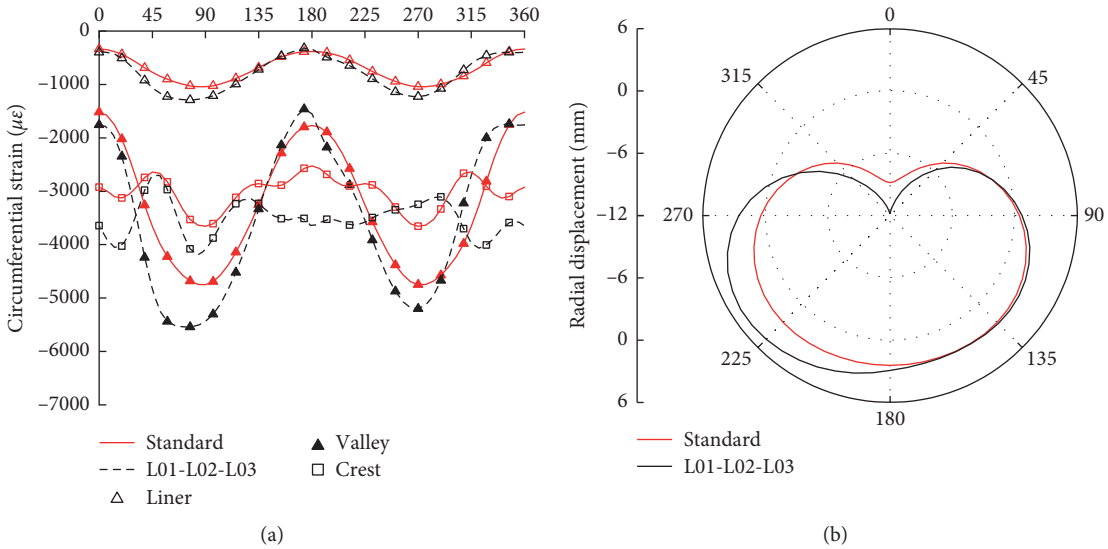

Figure 24: Distribution of (a) circumferential strain and (b) radial displacement when the left sides of Lay 01, Lay 02, and Lay 03 were loose.

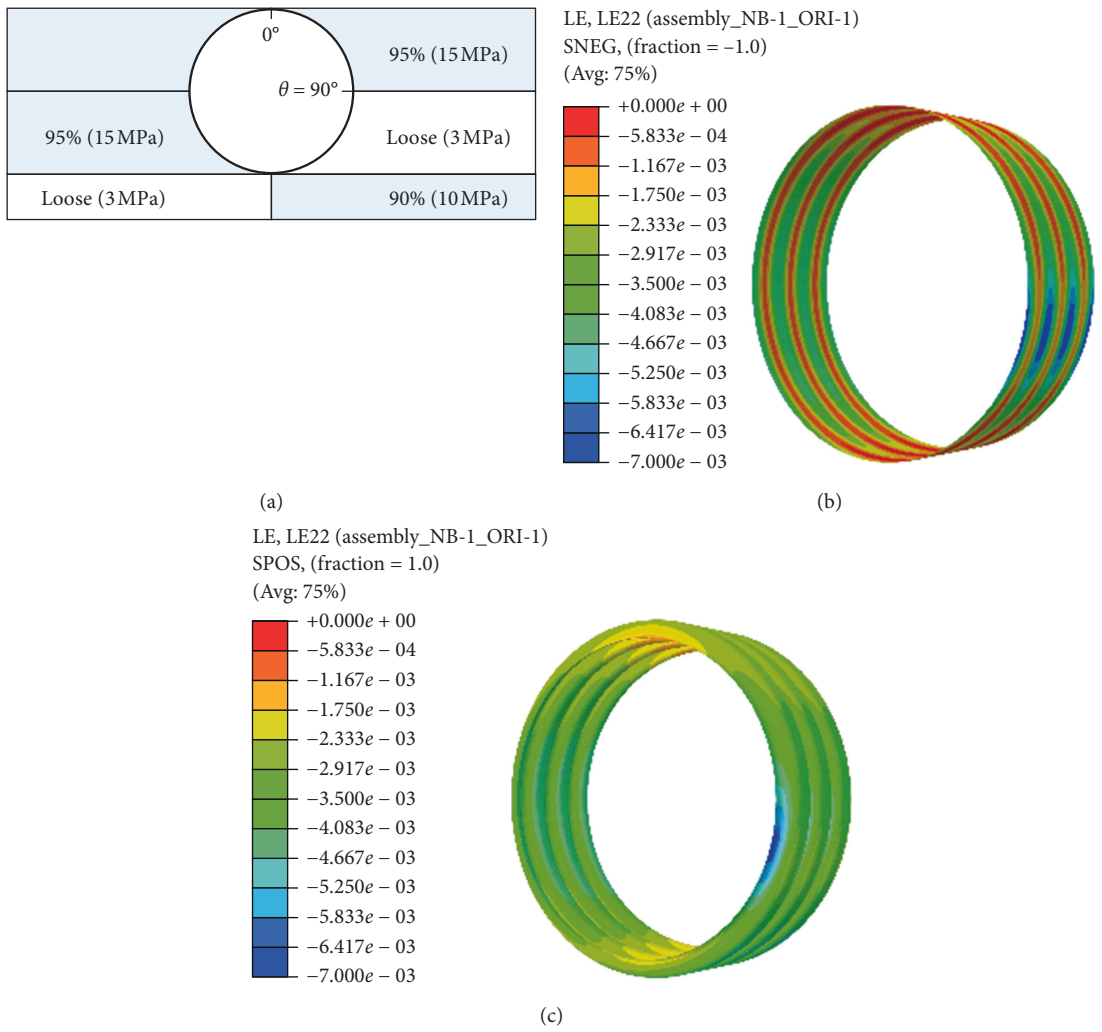

FIGURE 25: (a) Location of loose backfill; the circumference strain nephogram of the (b) interior wall and (c) exterior wall when the left side of Lay 01 and the right side of Lay 02 were loose.

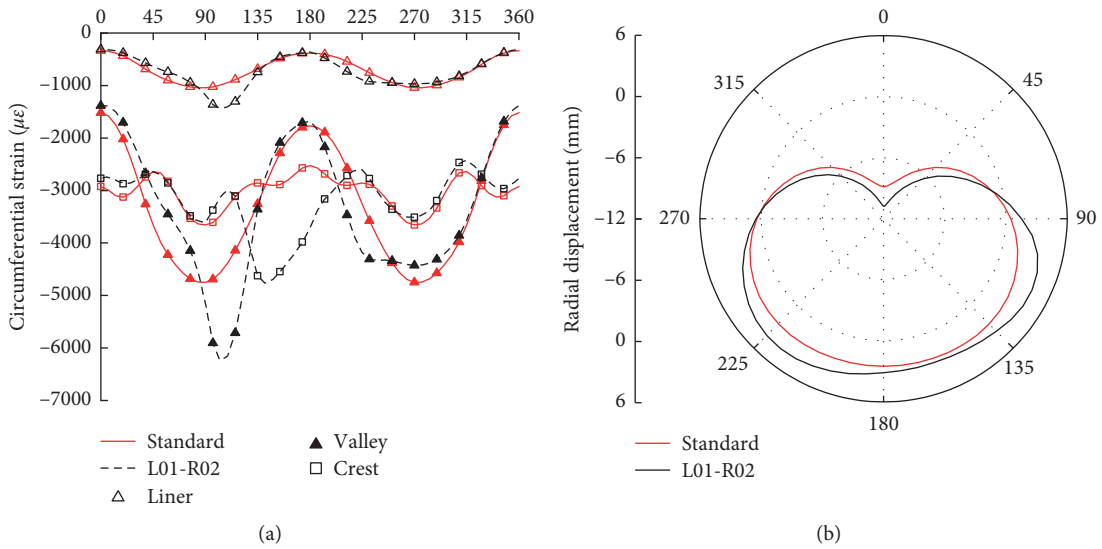

FIGURE 26: Distribution of (a) circumferential strain and (b) radial displacement when the left side of Lay 01 and the right side of Lay 02 were loose.

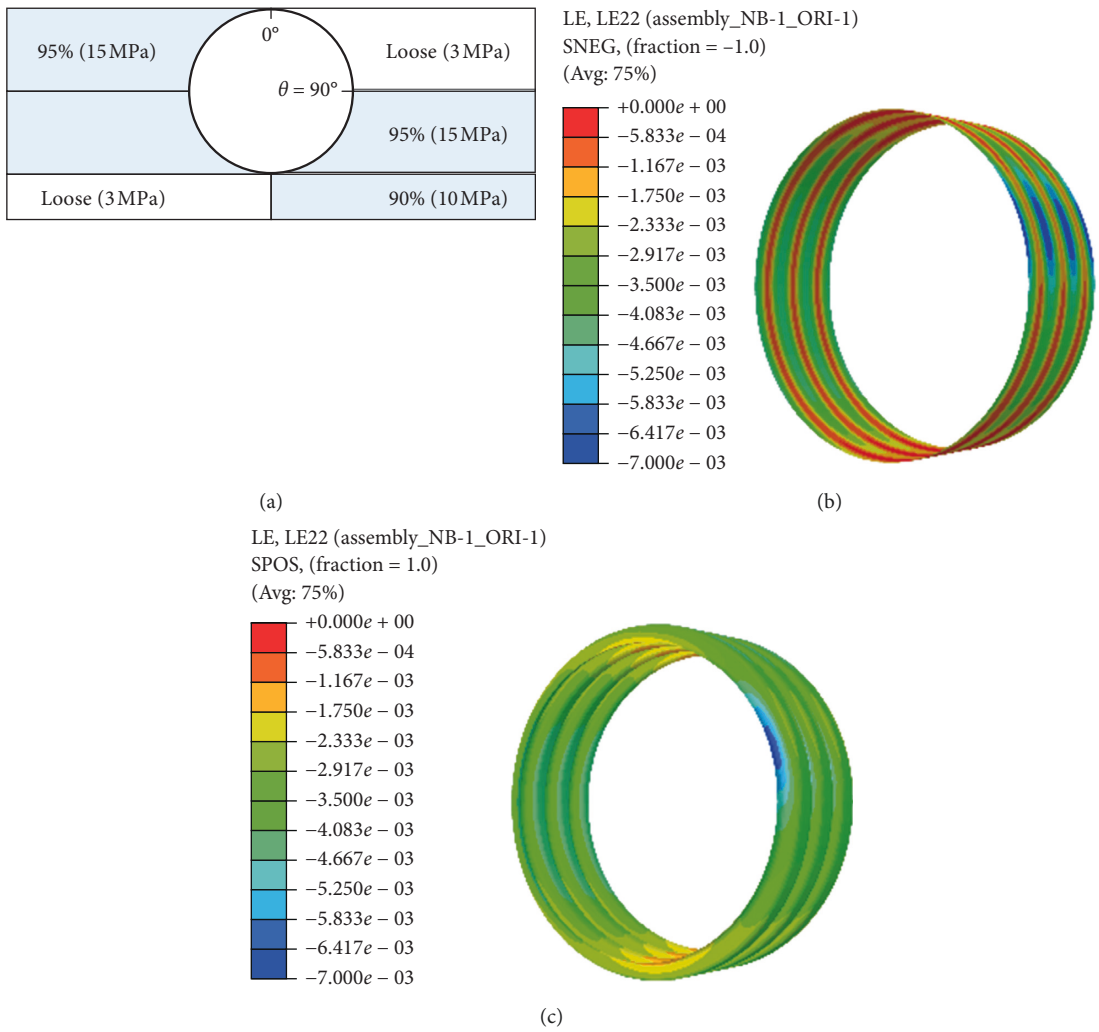

Figure 27: (a) Location of loose backfill; the circumference strain nephogram of the (b) interior wall and (c) exterior wall when the left side of Lay 01 and the right side of Lay 03 were loose.

remained constant at the above half region (i.e., 270°–90°) where it is contacted with the dense backfill, and the interior wall strain of the lower half region increases. Near the right-haunch, the circumferential strains of the interior wall reaches the maximum; the liner strain increases by 38%, the valley strain increases by 32%, and the difference between the strains at the liner and the valley increases by 30%, which had the greatest influence on crest circumferential strain at the invert; the crest strain increases by the poor support of the region. The maximum compression increases by 30% (the position moves from the springline to the haunch). In addition, the deformation profile is still "heart deformation" but the axial displacement magnitude is greater. The reason is that the loose backfill under the haunch led to the weakening of the support of pipe, and the weakness of the left base is exacerbated in this bad situation.

As can be seen from Figures 27 and 28, the circumferential strain at the liner or the valley increases in the region supported by the loose backfill when the backfill of left Lay 01 and right Lay 03 are loose. Near the right-springline, the maximum liner strain increases by 40% and the maximum valley strain increases by 33%. For the crest circumferential strain, the loose backfill was severely affected near the crown and the maximum occurred at the right-shoulder and increases by 19%. However, the radial displacement reduced from the shoulder to the springline and the displacement of the left side of the pipe increases.

Figures 29 and 30 plot the calculated value of the circumferential strain and displacement under the condition where the backfill of Lay 02 left and Lay 03 right are loose. The circumferential strains of the interior wall increase and decrease in the region around the loose and well-compacted backfill, respectively. There are two peak values of the valley circumferential strains in the two regions supported by loose backfill, and the magnitudes of the two peak values are almost equal. The change law of the liner circumferential strain is similar to that of the valley strain. The maximum strain of the liner and the valley increases by 48% and 39%, respectively. The position of the most prone to location buckling is near springline, and the displacement change at this point is also the greatest.

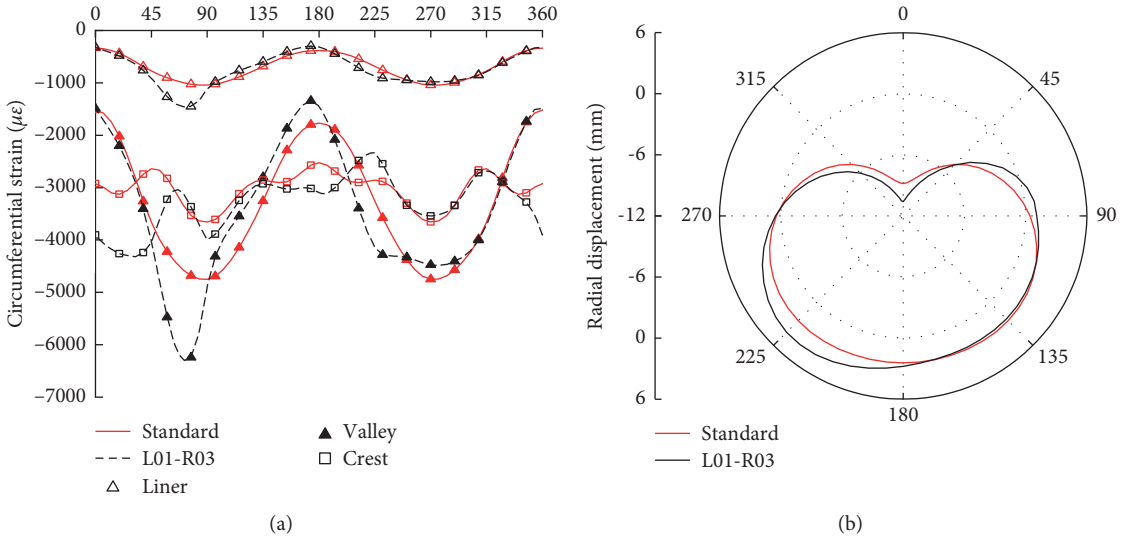

Figure 28: Distribution of (a) circumferential strain and (b) radial displacement when the left side of Lay 01 and the right side of Lay 03 were loose.

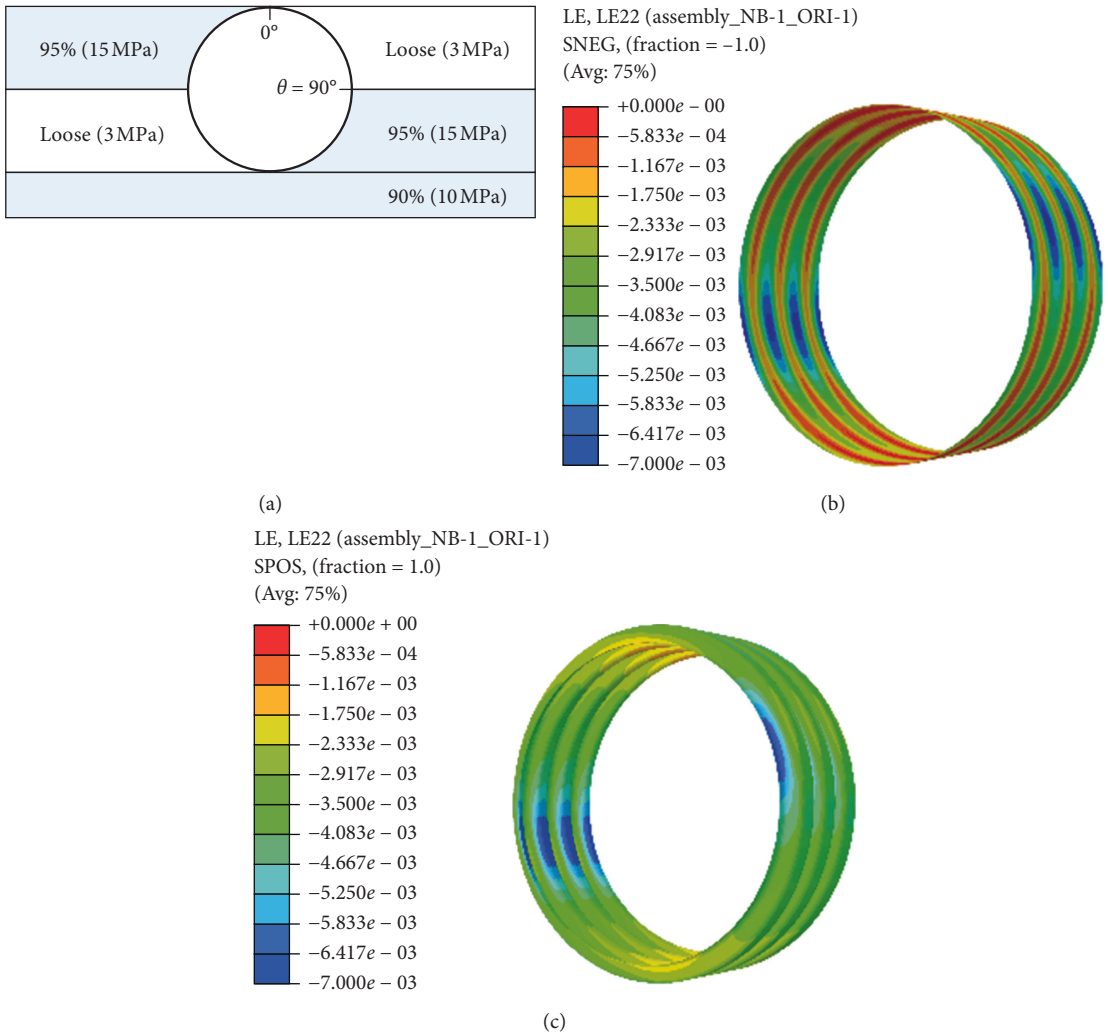

Figure 29: (a) Location of loose backfill: the circumference strain nephogram of the (b) interior wall and (c) exterior wall when the left side of Lay 02 and the right side of Lay 03 were loose.

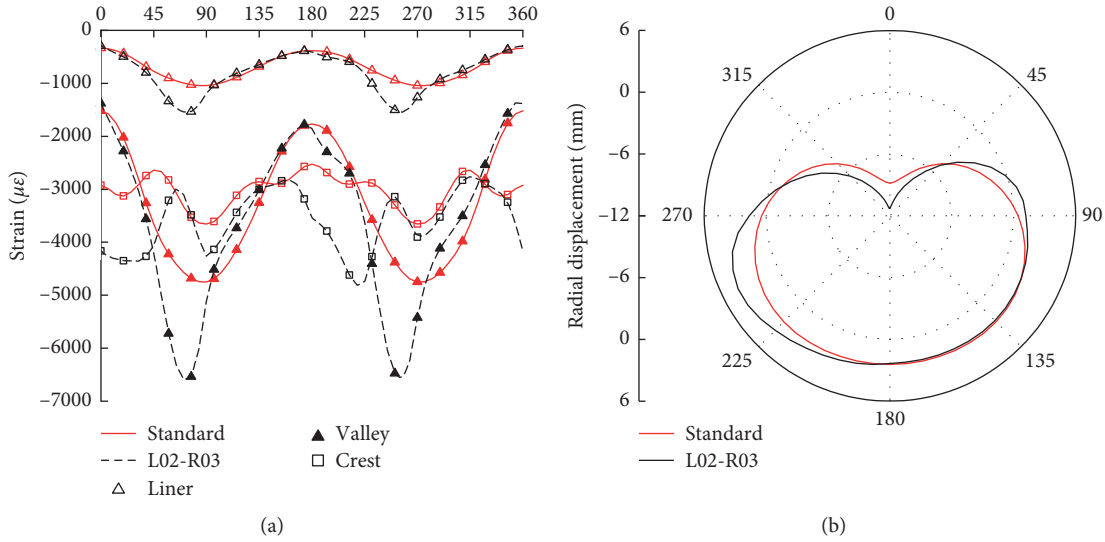

Figure 30: Distribution of (a) circumferential strain and (b) radial displacement when the left side of Lay 02 and the right side of Lay 03 were loose.

The response of the crest strain to backfill stiffness is more sensitive and complex. The distribution of the crest strain is completely different from that under standard compaction, and the standard strain is smaller. The strain changed mostly near the crown and the springline, and the maximum appears at the left-haunch and increased by 32%. In the regions supported by the loose backfill, the radial displacement increases greatly and the maximum value appears near the left-haunch.

The failure of the pipeline usually starts from the position of the maximum strain, and the local buckling is most likely to occur in the position of the maximum difference between the liner circumferential strain and the valley circumferential strain. Table 5 summarizes the increments of the maximum strain of pipe in different locations under the above ten backfilling conditions.

The response of the pipe to the loose backfill is related not only to the size of the region with loose backfill but also to the location of the region, and the location of the region with loose backfill is more critical than the size. It can be found that the pipe had higher requirements on the compaction of the backfill in the surrounding pipe (i.e., Lay 02 and Lay 03), especially the haunch backfill (i.e., Lay 02). In the case of loose local backfill, the maximum value of the liner circumferential strain is more susceptible than the change in the valley circumferential strain. However, for the base of the pipe, proper reduction of the stiffness of backfill can reduce the strain of the pipe. When Lay 02 and the backfill with the adjacent region are loose on the left side of the pipe, although the range of the backfill of low stiffness has expanded, the variation of the pipe strain maximum is reduced. When the loose region of the backfill is distributed on the left and the right, the asymmetry of backfill stiffness is enhanced and the maximum strain increment is greater than that when the left side of single-layer backfill is loose and had more possibilities of local buckling of pipe occurring.

Table 5: Increments of maximum circumferential strain of the pipe.

Condition	Crest (%)	Valley (%)	Liner (%)	Difference between valley strain and liner strain (%)
L01	0	0	0	0
L02	25	28	34	27
L03	18	26	33	27
L01-L02	5	13	16	12
L01-L03	20	28	23	20
L02-L03	15	14	22	13
L01-L02-L03	15	17	24	14
L01-R02	30	32	38	30
L01-R03	19	33	40	42
L02-R03	32	39	48	36

6. Conclusion

The paper compared the measured value and calculated value of the buried HDPE double-wall corrugated pipes, which showed that the three-dimensional finite element model can be effectively employed to calculate the pipe strain under the structure field. Based on the finite element model, it studied the strain distribution of the pipe under the exterior load. The following conclusions are obtained:

(1) The strain distribution trends of the liner and the valley are very similar, and the maximum strain of the interior wall often appears near the springline, which is the region most likely to be locally buckling.

(2) When the pipe is buried in the well-compacted soil, the most dangerous location of the exterior wall is the springline. Nevertheless, if the backfill is loose around the pipe, the most obvious change of the crest circumferential strain is near the crown or the invert.

(3) When there is a loose region in the backfill around the pipe, near the interface between the backfill loose

region and the well-compacted region, the maximum circumferential strain occurs frequently, and the point where the pipe radial displacement changes the most often coincides with the maximum point of the valley circumferential strain.

(4) The response of the pipe to the loose backfill is related not only to the size of the backfill loose region but also to the location of the region, and the location of the region with loose backfill is more critical than the size.

(5) The compaction of backfill under the haunch has the greatest influence on the strain state and deformation of the pipe. Therefore, in the actual construction process, it must be ensured that the compaction degree of the backfill in the region was good enough for specification requirements.

Data Availability

The figure and table data used to support the findings of this study are included within the article. In addition, the finite element models are available from the corresponding author upon request.

Conflicts of Interest

The authors declare that there are no conflicts of interest regarding the publication of this paper.

Acknowledgments

The authors acknowledge the financial support provided by the National Key Research and Development Program of China (No. 2016YFC0802400), the National Natural Science Foundation of China (No. 51978630, 51678536), the Program for Science and Technology Innovation Talents in Universities of Henan Province (Grant no. 19HASTIT043), the Outstanding Young Talent Research Fund of Zhengzhou University (1621323001), and the Program for Innovative Research Team (in Science and Technology) in University of Henan Province (18IRTSTHN007).

References

[1] GJBT-778, *Buried Plastic Drainage Pipe Construction (Chinese Standard)*, China Planning Press, Beijing, China, 2006.

[2] A. S. Dhar and I. D. Moore, "Liner buckling in profiled polyethylene pipes," *Geosynthetics International*, vol. 8, no. 4, pp. 303–326, 2001.

[3] J. Zhang, Z. Liang, and G. Zhao, "Mechanical behaviour analysis of a buried steel pipeline under ground overload," *Engineering Failure Analysis*, vol. 63, pp. 131–145, 2016.

[4] Z. Liang, Q. Yang, J. Zhang, and B. Zhu, "Mechanical analysis of buried polyethylene pipelines under ground overload," *Journal of Failure Analysis and Prevention*, vol. 19, no. 1, pp. 193–203, 2019.

[5] J. Zhang, Z. Liang, and C. Han, "Mechanical behaviour analysis of buried pressure pipeline crossing ground settlement zone," *International Journal of Pavement Engineering*, vol. 18, no. 7, pp. 608–621, 2017.

[6] J. Zhang and R. Xie, "Numerical analysis of mechanical behavior of buried pipes in subsidence area caused by underground mining," *Journal of Pressure Vessel Technology*, vol. 141, no. 2, Article ID 021703, 2019.

[7] M. Zhou, F. Wang, Y.-J. Du, and M. D. Liu, "Laboratory evaluation of buried high-density polyethylene pipes subjected to localized ground subsidence," *Acta Geotechnica*, vol. 14, no. 4, pp. 1081–1099, 2019.

[8] J. Zhang, L. Zhang, and Z. Liang, "Buckling failure of a buried pipeline subjected to ground explosions," *Process Safety and Environmental Protection*, vol. 114, pp. 36–47, 2018.

[9] Y. Guo, C. Liu, D. Wang, and R. He, "Numerical study and safety spacing of buried parallel gas pipelines: a study based on TNT equivalent method," *International Journal of Pressure Vessels and Piping*, vol. 168, pp. 246–257, 2018.

[10] J. Zhang, Z. Liang, and C. Han, "Numerical simulation of pipeline deformation caused by rockfall impact," *The Scientific World Journal*, vol. 2014, Article ID 161898, 10 pages, 2014.

[11] B. Wang and D. S. Cavers, "A simplified approach for rockfall ground penetration and impact stress calculations," *Landslides*, vol. 5, no. 3, pp. 305–310, 2008.

[12] J. Kang, "Finite element analysis for deeply buried concrete pipes in proposed imperfect trench installations with expanded polystyrene (EPS) foams," *Engineering Structures*, vol. 189, pp. 286–295, 2019.

[13] M. Al-Naddaf, J. Han, C. Xu, and S. M. Rahmaninezhad, "Effect of geofoam on vertical stress distribution on buried structures subjected to static and cyclic footing loads," *Journal of Pipeline Systems Engineering and Practice*, vol. 10, no. 1, Article ID 04018027, 2019.

[14] B. Li, H. Fang, H. He, K. Yang, C. Chen, and F. Wang, "Numerical simulation and full-scale test on dynamic response of corroded concrete pipelines under multi-field coupling," *Construction and Building Materials*, vol. 200, pp. 368–386, 2019.

[15] H. Fang, B. Li, F. Wang, Y. Wang, and C. Cui, "The mechanical behaviour of drainage pipeline under traffic load before and after polymer grouting trenchless repairing," *Tunnelling and Underground Space Technology*, vol. 74, pp. 185–194, 2018.

[16] J. Zhang, Y. Xiao, and Z. Liang, "Mechanical behaviors and failure mechanisms of buried polyethylene pipes crossing active strike-slip faults," *Composites Part B: Engineering*, vol. 154, pp. 449–466, 2018.

[17] W. Wang, L. Wang, D. H. Ma, and J. Y. Su, "3D FEM analysis of buried pipeline affected by excavation of adjacent foundation pits under different protection measures," *Journal of Beijing University of Technology*, vol. 35, no. 7, pp. 939–946, 2009.

[18] J. Zhang, R. Xie, and H. Zhang, "Mechanical response analysis of the buried pipeline due to adjacent foundation pit excavation," *Tunnelling and Underground Space Technology*, vol. 78, pp. 135–145, 2018.

[19] R. W. I. Brachman, I. D. Moore, and S. M. Munro, "Compaction effects on strains within profiled thermoplastic pipes," *Geosynthetics International*, vol. 15, no. 2, pp. 72–85, 2008.

[20] S. L. Gassman, A. J. Schroeder, and R. P. Ray, "Field performance of high density polyethylene culvert pipe," *Journal of Transportation Engineering*, vol. 131, no. 2, pp. 160–167, 2005.

[21] A. Marston and A. O. Anderson, *The Theory of Loads on Pipes in Ditches: And Tests of Cement and Clay Drain Tile and Sewer Pipe*, Vol. 31, Iowa State College of Agriculture and Mechanic Arts, Ames, IA, USA, 1913.

[22] M. G. Spangler and G. E. Shafer, "The structural design of flexible pipe culverts," in *Proceedings of the Highway Research Board*, vol. 17, Washington, DC, USA, November 1938.

[23] A. Howard, "Load-deflection field test of 27-inch (675-mm) PVC (polyvinyl chloride) pipe," in *Buried Plastic Pipe Technology*, ASTM International, West Conshohocken, PA, USA, 1990.

[24] E. Faragher, C. D. F. Rogers, and P. R. Fleming, "Laboratory determination of soil stiffness data for buried plastic pipes," *Transportation Research Record: Journal of the Transportation Research Board*, vol. 1624, no. 1, pp. 231–236, 1998.

[25] S. Sargand, T. Masada, G. Hazen, and D. Schehl, "Field verification of structural performance of thermoplastic pipe under deep backfill conditions," NASA STI/Recon Technical Report N, NASA, Washington, DC, USA, 2002.

[26] T. J. McGrath, E. T. Selig, M. C. Webb, and G. V. Zoladz, "Pipe interaction with the backfill envelope," FHWA, Washington, DC, USA, No. FHWA-RD-98-191, 1999.

[27] A. S. Dhar, I. D. Moore, and T. J. McGrath, "Two-dimensional analyses of thermoplastic culvert deformations and strains," *Journal of Geotechnical and Geoenvironmental Engineering*, vol. 130, no. 2, pp. 199–208, 2004.

[28] D. S. Al-Abri and Y. E. Mohamedzein, "Performance of plastic pipes installed in dune sand," in *Proceedings of the Pipelines 2010: Climbing New Peaks to Infrastructure Reliability-Renew, Rehab, and Reinvest*, pp. 402–414, Keystone, CO, USA, August 2010.

[29] F. Wang, Y. J. Du, M. Zhou, and Y. J. Zhang, "Experimental study of the effects produced by a backfilling process on full-scale buried corrugated HDPE pipes in fine-grained soils," *Journal of Pipeline Systems Engineering and Practice*, vol. 7, no. 1, Article ID 05015001, 2015.

[30] T. J. M. McGrath, S. J. DelloRusso, and J. Boynton, "Performance of thermoplastic culvert pipe under highway vehicle loading," in *Proceedings of the Pipelines 2002: Beneath Our Feet: Challengers and Solutions*, Cleveland, OH, USA, August 2002.

[31] M. A. Noor and A. S. Dhar, "Three-dimensional response of buried pipe under vehicle loads," in *Proceedings of the International Conference on 2003 Pipeline Engineering and Construction*, vol. 1, American Society of Civil Engineers, Baltimore, MA, USA, July 2003.

[32] S. M. Tafreshi and O. Khalaj, "Analysis of repeated-load laboratory tests on buried plastic pipes in sand," *Soil Dynamics and Earthquake Engineering*, vol. 31, no. 1, pp. 1–15, 2011.

[33] CJJ 143-2010, *Technical Specification for Buried Plastic Pipeline of Sewer Engineering (Chinese Standard)*, China Building Industry Press, Beijing, China, 2010.

[34] T. J. McGrath, "Design method for flexible pipe," A Rep. to the AASHTO Flexible Culvert Liaison Committee, Sinpson Gumpertz & Heger Inc., Arlington, MA, USA, 1998.

[35] R. K. Watkins, E. Szpak, and W. Allman, "Structural design of polyethylene pipes subjected to external loads," Utah State University, Logan, UT, USA, 1974.

[36] D. Cebon, "Interaction between heavy vehicles and roads (no. 930001)," in *Proceedings of the SAE Technical Paper Series*, Colorado Springs, CO, USA, March 1993.

[37] I. D. Moore and F. Hu, "Linear viscoelastic modelling of profiled high density polyethylene pipe," *Canadian Journal of Civil Engineering*, vol. 23, no. 2, pp. 395–407, 1996.

[38] C. D. F. Rogers, "Some observations on flexible pipe response to load," *Transportation Research Record (1191)*, Transportation Research Board, Washington, DC, USA, 1988.

[39] C. D. F. Rogers, P. R. Fleming, and R. Talby, "Use of visual methods to investigate influence of installation procedure on pipe-soil interaction," *Transportation Research Record: Journal of the Transportation Research Board*, vol. 1541, no. 1, pp. 76–85, 1996.

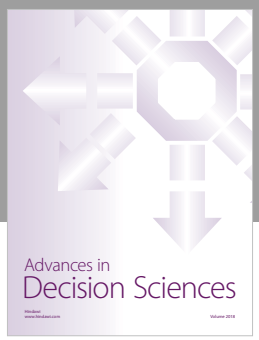

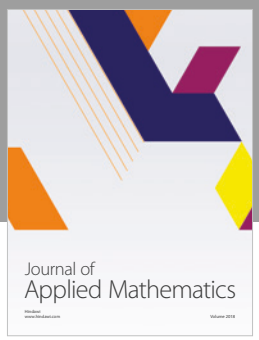

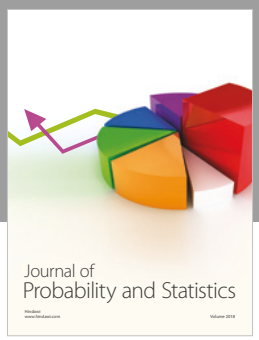

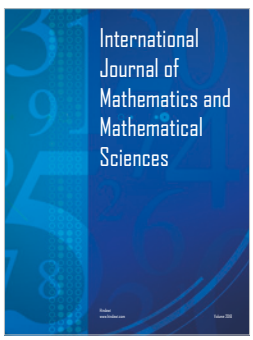

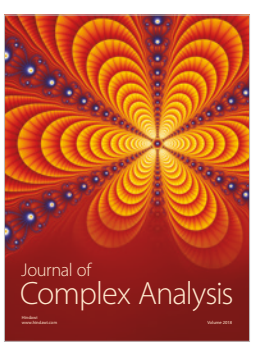

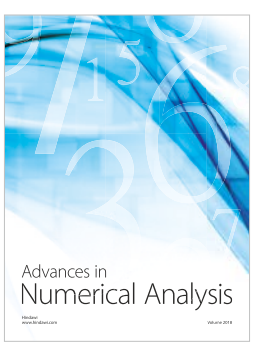

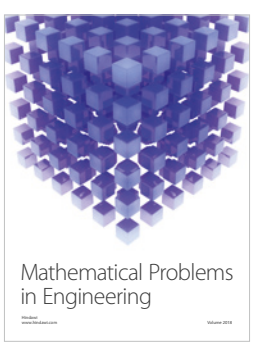

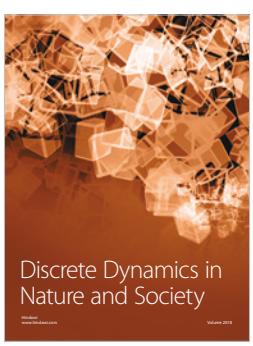

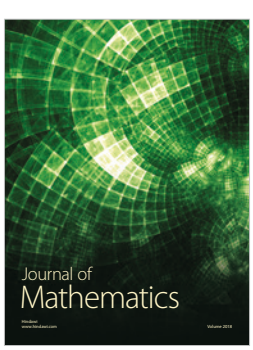

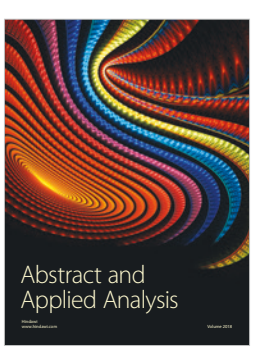

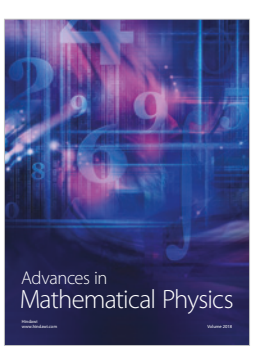

Hindawi

Submit your manuscripts at
www.hindawi.com